



UNIVERSIDADE FEDERAL DO RIO GRANDE DO NORTE
CENTRO DE CIÊNCIAS EXATAS E DA TERRA
PROGRAMA DE PÓS-GRADUAÇÃO EM GEODINÂMICA E GEOFÍSICA

DISSERTAÇÃO DE MESTRADO

**INTEGRANDO ESTRATIGRAFIA, PETROFÍSICA E REDE DE
FRATURAS CARSTIFICADAS EM UM MODELO DIGITAL 3D
UNIFICADO: EXEMPLO DA CAVERNA CRISTAL (CRÁTON SÃO
FRANCISCO, NORDESTE DO BRASIL).**

Autor:

JOÃO VICTOR FREIRE PEREIRA

Orientador:

PROF. DR. WALTER EUGÉNIO DE MEDEIROS

Dissertação nº 277/PPGG

Novembro de 2022

Natal/RN, Brasil

JOÃO VICTOR FREIRE PEREIRA

**INTEGRANDO ESTRATIGRAFIA, PETROFÍSICA E REDE DE
FRATURAS CARSTIFICADAS EM UM MODELO DIGITAL 3D
UNIFICADO: EXEMPLO DA CAVERNA CRISTAL (CRÁTON SÃO
FRANCISCO, NORDESTE DO BRASIL).**

Dissertação apresentada em 24 de Novembro de 2022 ao Programa de Pós-Graduação em Geodinâmica e Geofísica (PPGG) da Universidade Federal do Rio Grande do Norte (UFRN) como requisito à obtenção do Título de Mestre em Geodinâmica e Geofísica, Área de Concentração Geodinâmica.

BANCA EXAMINADORA:

PROF. DR. WALTER EUGÊNIO DE MEDEIROS
Presidente e orientador (PPGG-UFRN)

PROF. DR. FRANCISCO CÉZAR COSTA NOGUEIRA
Membro externo (UFCG)

PROF. DR. DAVID LINO VASCONCELOS
Membro externo (UFCG)

Universidade Federal do Rio Grande do Norte - UFRN
Sistema de Bibliotecas - SISBI

Catalogação de Publicação na Fonte. UFRN - Biblioteca Setorial Prof. Ronaldo Xavier de Arruda - CCET

Pereira, João Victor Freire.

Integrando estratigrafia, petrofísica e rede de fraturas
carstificadas em um modelo digital 3D unificado: exemplo da
Caverna Cristal (Cráton São Francisco, Nordeste do Brasil) /
João Victor Freire Pereira. - 2022.

63f.: il.

Dissertação (Mestrado) - Universidade Federal do Rio Grande
do Norte, Centro de Ciências Exatas e da Terra, Programa de Pós-
Graduação em Geodinâmica e Geofísica. Natal, 2022.
Orientador: Prof. Dr. Walter Eugênio de Medeiros.

1. Geodinâmica - Dissertação. 2. Modelo digital de
afloramento - Dissertação. 3. Redes de fraturas discretas -
Dissertação. 4. Carste - Dissertação. 5. Reservatórios
carbonáticos - Dissertação. I. Medeiros, Walter Eugênio de. II.
Título.

RN/UF/CCET

CDU 551.2/.3

Resumo

Os DOMs (*Digital Outcrop Models* ou Modelos Digitais de Afloramento) são ferramentas amplamente utilizadas em investigações geológicas e estão em constante desenvolvimento. Contrastando com sua ampla utilização, o potencial dos DOMs ainda é subutilizado em relação à integração com outros dados. Apresentamos aqui uma abordagem integrativa, combinando um DOM com informações estratigráficas e petrofísicas, além de dados de distribuição de fraturas e dissolução cárstica. Aberturas de fraturas alargadas por dissolução cárstica são implementadas em uma Rede de Fraturas Discretas (DFN, do inglês) para gerar uma Rede de Fraturas Carstificadas Discretas (DFKN), a partir da qual é possível compor diferentes cenários de intensidade de carstificação. O DOM utilizado é baseado em dados fotogramétricos obtidos em um segmento da Caverna Cristal, a qual desenvolveu-se em carbonatos Mesoproterozoicos da Formação Caboclo, no Grupo Chapada Diamantina, Cráton São Francisco, Nordeste do Brasil. Esta caverna é entendida como um afloramento análogo estrutural e diagenético para os reservatórios carbonáticos do Pré-sal brasileiro. O Modelo Integrativo descrito aqui combina tanto elementos determinísticos (estratigrafia e petrofísica) quanto estocásticos (DFN e DFKN). Neste modelo, a estratigrafia do afloramento é reproduzida como 22 camadas tabulares e paralelas, as quais foram populadas com medidas de porosidade, permeabilidade e resistência à compressão uniaxial. Recorrendo a uma abordagem estocástica, obteve-se um DFN 3D através da resolução do problema inverso da esteoreologia, honrando as medidas estatísticas dos traços de fratura (lei de potência e persistência P_{21}) medidos nas paredes e teto da caverna. Parâmetros petrofísicos podem ser alterados facilmente no Modelo Integrativo, também sendo possível modificar a lei de potência que correlaciona a abertura ao comprimento das fraturas, para implementar diferentes estágios de carstificação das aberturas das fraturas. Como resultado, diferentes cenários de porosidades primária e secundária podem ser obtidos, os quais podem ser utilizados em simulações de fluxo de fluido, facilitando assim o entendimento dos múltiplos fatores que afetam o comportamento dos reservatórios carbonáticos.

Palavras-chave: Modelo Digital de Afloramento; Redes de Fraturas Discretas; carste; reservatórios carbonáticos.

Abstract

Digital Outcrop Models (DOMs) are visual representations of geological sites in a virtual environment. DOMs are constantly evolving and widely used tools for geological investigations. However, in contrast with their broad applications, the full potential of DOMs is still underexplored in terms of their integration with other data. We present an integrative approach by combining a DOM with stratigraphic, petrophysical, fracture distribution and karst dissolution information into a single 3D georeferenced digital model. Fracture aperture enlargement due to karstic dissolution are implemented on a Discrete Fracture Network (DFN) to generate a Discrete Fracture and Karst Network (DFKN), where it is possible to compose different karstification intensity scenarios. The used DOM is based on photogrammetric data obtained inside a segment of the Cristal Cave. This cave developed in Mesoproterozoic carbonate rocks of the Caboclo Formation, in the Chapada Diamantina Group, São Francisco Craton, Northeastern Brazil, and has been used as a structural and diagenetic outcrop analogue for the Brazilian pre-salt carbonate reservoirs. The described Integrative Model combines both deterministic (stratigraphy and petrophysics) and stochastic (DFN and DFKN) elements. The framework of the Integrative Model reproduces the stratigraphy of the outcrop as 22 parallel layers, which were populated with porosity, permeability and uniaxial compressive strength measurements. Resorting to a stochastic approach, we obtained a 3D DFN by solving the stereology inverse problem, where statistical measurements of the fracture traces (power law and P_{21} persistences) on the walls and ceiling of the cave are honored. Petrophysical parameters of the Integrative Model can be easily changed, while it is also possible to modify the power law that relates aperture and fracture length to implement different karstification stages of the fracture apertures. As a result, different scenarios of primary and secondary porosities can be easily composed, which can be used in fluid flow simulations, thus facilitating the understanding of the multiple factors affecting the behavior of carbonate reservoirs.

Keywords: Digital Outcrop Model; Discrete Fracture Network; karst; carbonate reservoirs.

Agradecimentos

Às entidades patrocinadoras e gerenciadoras do Projeto CristalDOM, em específico à Petrobras e à Funpec pelo financiamento do projeto e pela remuneração pessoal através da bolsa de mestrado.

À Universidade Federal do Rio Grande do Norte e ao Programa de Pós-Graduação em Geodinâmica e Geofísica (PPGG) pelas estruturas física e organizacional, sem as quais este trabalho não seria possível. Agradecemos também ao Instituto Nacional de Ciência e Tecnologia em Geofísica do Petróleo (INCT-GP/CNPq/CAPES) pelo uso da infraestrutura computacional.

Ao Prof. Dr. Walter E. de Medeiros, meu orientador, pelo apoio irrestrito e incentivo ao longo dessa jornada.

Aos membros da banca, Prof. Dr. David Lino e Prof. Dr. Francisco Cézar Nogueira, pelas importantes indicações e melhorias na dissertação.

Aos Prof. Dr. Francisco Hilário R. Bezerra, coordenador do Projeto CristalDOM, e a Dra. Maria Osvalneide Lucena pela cuidadosa condução do projeto e pelas assistências burocráticas.

Às equipes de campo, incluindo professores parceiros, colegas de outras instituições, guias e motoristas que prezaram pela execução plena e segura das atividades de campo.

À Dra. Juliana Lopes pelas discussões enriquecedoras e ao Prof. Dr. Renato Dantas pela prestatividade e acompanhamento meticoloso durante toda as etapas desta pesquisa.

Aos caríssimos colegas de laboratório (LABSIS), que recorrentemente tornaram a rotina de trabalho mais amena.

Aos amigos pessoais e familiares pela compreensão em momentos de ausência e apoio pleno nessa trajetória.

Finalmente, agradeço a todos que contribuíram direta ou indiretamente para a realização deste trabalho.

Sumário

Resumo	i
Abstract	iii
Sumário	v
1 Introdução	1
1.1 Apresentação	1
1.2 Justificativa	3
1.3 Contextualização Geológica da Caverna Cristal	4
Referências bibliográficas	7
2 Estado da Arte dos Conceitos-chave	8
2.1 DOM - Modelos Digitais de Afloramento	8
2.2 DFN - Redes de Fraturas Discretas	10
Referências bibliográficas	15
3 Manuscrito Submetido: “<i>Integrating stratigraphy, petrophysics and karstified fracture network into a single 3D Digital Model: Example from the Cristal (São Francisco Craton, NE/Brazil).</i>”	16

Capítulo 1

Introdução

1.1 Apresentação

Esta dissertação de mestrado foi desenvolvida sob a orientação do Prof. Dr. Walter Eugênio de Medeiros e sua elaboração é um requisito necessário para a obtenção do título de Mestre em Geodinâmica e Geofísica, pelo Programa de Pós-graduação em Geodinâmica e Geofísica da Universidade Federal do Rio Grande do Norte (UFRN).

A pesquisa reportada nesta dissertação desenvolveu-se no âmbito do Projeto CristalDOM - "Modelo Digital 3D da Gruta Cristal I, Morro do Chapéu - Bahia", o qual é financiado pela Petrobras e sediado na UFRN sob coordenação do Prof. Dr. Francisco Hilário Rego Bezerra. Este projeto conta com colaboradores de diversas universidades, tendo como objetivo a geração de modelos digitais de afloramento (do inglês, DOM) a partir de dados fotogramétricos da Caverna Cristal, localizada no Cráton São Francisco, Nordeste do Brasil. As linhas de pesquisa do projeto se desdobram em várias direções, complementando a geração dos modelos com caracterizações estruturais, estratigráficas e sedimentológicas.

O cerne do trabalho executado trata-se da elaboração de um Modelo Integrativo que combina dados estruturais, estratigráficos, litológicos e petrofísicos em um ambiente digital 3D unificado e georreferenciado. O Modelo Integrativo é centrado no DOM do Acesso 1 da Caverna Cristal (Figura 1.1), de forma que o DOM além de ser utilizado como ferramenta de visualização, também é empregado na interpretação de dados estruturais e no referenciamento dos demais conjuntos de dados no ambiente 3D.

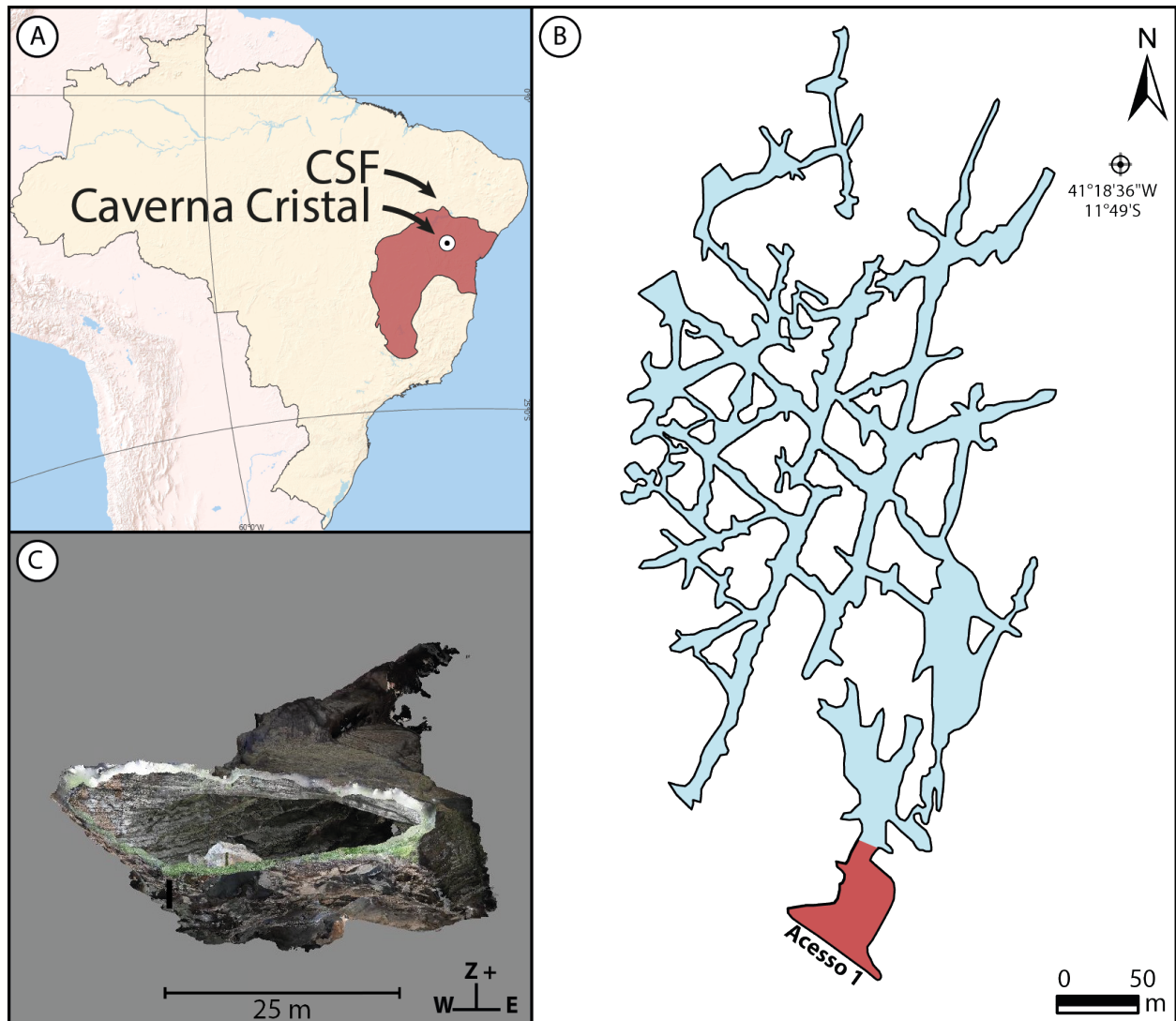


Figura 1.1: Contextualização da Caverna Cristal. A) Limites e posicionamento relativo do Cráton São Francisco em relação ao Brasil. B) Mapa da Caverna Cristal ressaltando a localização do Acesso 1. C) DOM do Acesso 1, notar referência espacial no canto inferior direito.

1.2 Justificativa

Rochas carbonáticas podem apresentar diferentes condições de permeabilidade e porosidade primária e secundária (Aydin, 2000; Bohnsack et al., 2020; Shen et al., 2015). Em escala de reservatório, essa variação intrínseca às rochas carbonáticas somada à ocorrência de processos estruturais e diagenéticos, a exemplo de fraturamento (Guerriero et al., 2013), silicificação (You et al., 2018) e dissolução (Popov et al., 2009), compõem um cenário de alta complexidade. Tendo em vista que a escala de reservatório é um fator limitante às formas de investigação direta desses processos, os estudos de afloramentos análogos ganham relevância nesse contexto e se fazem imprescindíveis para uma melhor compreensão da complexidade dos reservatórios carbonáticos (Howell et al., 2014; Wennberg et al., 2007). Neste sentido, destacamos o uso dos *Digital Outcrop Models* (DOMs) e dos *Discrete Fracture Networks* (DFNs), os quais são ferramentas amplamente utilizadas nesses estudos. Os DOMs são representações de afloramentos geológicos no ambiente digital (Bellian et al., 2005), enquanto que os DFNs referem-se a reproduções virtuais, estocásticas ou determinísticas, de redes de fraturas (Lei et al., 2017). Adicionalmente, trataremos também da implementação do alargamento por dissolução cárstica da abertura das fraturas dos DFNs, a qual é referida por *Discrete Fracture and Karst Networks* (DFKN) (Lopes et al., 2021). Os conceitos elencados são sumarizados no Capítulo 2.

Em contraponto à sua ampla utilização, essas ferramentas constantemente são empregadas de forma isolada entre si e também em relação aos dados litológicos, estratigráficos e petrofísicos. Entende-se, nesse caso, que essa abordagem não usa todo o potencial desses recursos e que a aplicação de metodologias integrativas ainda é uma fronteira a ser explorada (Marques Jr et al., 2020). Visando a preencher essa lacuna, desenvolvemos um Modelo Integrativo tomando como base o DOM do Acesso 1 da Caverna Cristal (Figura 1.1). Nessa abordagem, o DOM é utilizado para georreferenciar e combinar elementos determinísticos (estratigrafia e petrofísica) e estocásticos (DFN e DFKN) em um ambiente 3D georreferenciado. Como resultado, temos um produto digital adequado à elaboração de modelos estáticos, utilizados por engenheiros em simulações de fluxo de fluido. Nesse contexto, o Modelo Integrativo permite ainda a composição de diferentes cenários de porosidades primária e secundária, através da respectiva alteração das medidas petrofísicas das

camadas e dos parâmetros estatísticos dos DFN e DFKN. Deste modo, há um encurtamento considerável do caminho entre o dado bruto de afloramento e o modelo estático, facilitando o fluxo de trabalho entre o geólogo/geofísico e o engenheiro.

1.3 Contextualização Geológica da Caverna Cristal

O presente trabalho tem um caráter metodológico e utiliza a Caverna Cristal como um exemplo de campo para suportar o desenvolvimento da nossa abordagem. A Caverna Cristal é uma rede cárstica com 6.7 km de extensão (Figura 1.1), localizada no município de Morro do Chapéu-BA e inclusa no Cráton São Francisco, região Nordeste do Brasil. Seu desenvolvimento se dá em rochas carbonáticas Mesoproterozoicas da Formação Caboclo (Figura 1.2), Grupo Chapada Diamantina, Supergrupo Espinhaço.

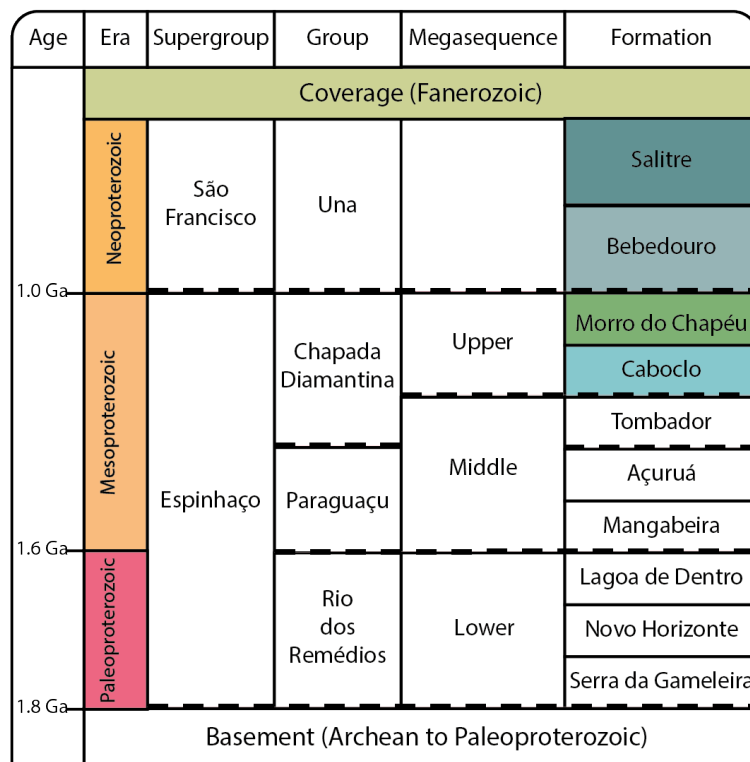


Figura 1.2: Coluna estratigráfica da região da Chapada Diamantina. A Caverna Cristal desenvolve-se nas unidades carbonáticas da Formação Caboclo, Grupo Chapada Diamantina, depositadas durante o Mesoproterozoico.

Descrições geológicas da Caverna Cristal destacam a ocorrência de estromatólitos (Ferronatto et al., 2021; Srivastava & Rocha, 2002), enquanto outros trabalhos traçam paralelos relevantes

entre os processos de silicificação, dissolução e fraturamento ocorrentes na caverna e os reservatórios carbonáticos do pré-sal brasileiro, considerando-a um afloramento análogo aos referidos reservatórios (La Bruna et al., 2021; Souza et al., 2021).

Referências Bibliográficas

- Aydin, A., 2000, Fractures, faults, and hydrocarbon entrapment, migration and flow: Marine and Petroleum Geology, **17**, 797–814.
- Bellian, J. A., C. Kerans, & D. C. Jennette, 2005, Digital outcrop models: applications of terrestrial scanning lidar technology in stratigraphic modeling: Journal of Sedimentary Research, **75**, 166–176.
- Bohnsack, D., M. Potten, D. Pfrang, P. Wolpert, & K. Zosseder, 2020, Porosity–permeability relationship derived from Upper Jurassic carbonate rock cores to assess the regional hydraulic matrix properties of the Malm reservoir in the South German Molasse Basin: Geothermal Energy, **8**, 1–47.
- Ferronatto, J. P. F., C. M. dos Santos Scherer, G. B. Drago, A. G. Rodrigues, E. G. de Souza, A. D. dos Reis, M. B. Bállico, C. Kifumbi, & C. L. Cazarin, 2021, Mixed carbonate-siliciclastic sedimentation in a mesoproterozoic storm-dominated ramp: Depositional processes and stromatolite development: Precambrian Research, **361**, 106240.
- Guerriero, V., S. Mazzoli, A. Iannace, S. Vitale, A. Carravetta, & C. Strauss, 2013, A permeability model for naturally fractured carbonate reservoirs: Marine and Petroleum Geology, **40**, 115–134.
- Howell, J. A., A. W. Martinius, & T. R. Good, 2014, The application of outcrop analogues in geological modelling: a review, present status and future outlook: Geological Society, London, Special Publications, **387**, 1–25.
- La Bruna, V., F. H. Bezerra, V. H. Souza, R. P. Maia, A. S. Auler, R. E. Araujo, C. L. Cazarin, M. A. Rodrigues, L. C. Vieira, & M. O. Sousa, 2021, High-permeability zones in folded and faulted silicified carbonate rocks – Implications for karstified carbonate reservoirs: Marine and Petroleum Geology, **128**, 105046.
- Lei, Q., J.-P. Latham, & C.-F. Tsang, 2017, The use of discrete fracture networks for modelling

- coupled geomechanical and hydrological behaviour of fractured rocks: Computers and Geotechnics, **85**, 151–176.
- Lopes, J. A. G., W. E. Medeiros, V. La Bruna, A. Lima, F. H. R. Bezerra, & D. J. Schiozer, 2021, Advancements towards DFKN modelling: Incorporating fracture enlargement resulting from karstic dissolution in discrete fracture networks: Journal of Petroleum Science and Engineering, **209**, 109944.
- Marques Jr, A., R. K. Horota, E. M. de Souza, L. Kupssinskü, P. Rossa, A. S. Aires, L. Bachi, M. R. Veronez, L. Gonzaga Jr, & C. L. Cazarin, 2020, Virtual and digital outcrops in the petroleum industry: A systematic review: Earth-Science Reviews, **208**, 103260.
- Popov, P., G. Qin, L. Bi, Y. Efendiev, Z. Kang, & J. Li, 2009, Multiphysics and Multiscale Methods for Modeling Fluid Flow Through Naturally Fractured Carbonate Karst Reservoirs: SPE Reservoir Evaluation & Engineering, **12**, 218–231.
- Shen, A., Z. Wenzhi, H. Anping, S. Min, C. Yana, & W. Xiaofang, 2015, Major factors controlling the development of marine carbonate reservoirs: Petroleum Exploration and Development, **42**, 597–608.
- Souza, V. H., F. H. Bezerra, L. C. Vieira, C. L. Cazarin, & J. A. Brod, 2021, Hydrothermal silicification confined to stratigraphic layers: Implications for carbonate reservoirs: Marine and Petroleum Geology, **124**, 104818.
- Srivastava, N. K., & A. J. D. Rocha, 2002, Fazenda Cristal, BA - Estromatólitos Mesoproterozóicos, *in* Sítios Geológicos e Paleontológicos do Brasil: Serviço Geológico do Brasil, 11, 87–93.
- Wennberg, O. P., M. Azizzadeh, A. A. M. Aqrabi, E. Blanc, P. Brockbank, K. B. Lyslo, N. Pickard, L. D. Salem, & T. Svånå, 2007, The Khaviz Anticline: an outcrop analogue to giant fractured Asmari Formation reservoirs in SW Iran: Geological Society, London, Special Publications, **270**, 23–42.
- You, D., J. Han, W. Hu, Y. Qian, Q. Chen, B. Xi, & H. Ma, 2018, Characteristics and formation mechanisms of silicified carbonate reservoirs in well SN4 of the Tarim Basin: Energy Exploration & Exploitation, **36**, 820–849.

Capítulo 2

Estado da Arte dos Conceitos-chave

O Modelo Integrativo, elaborado nesta pesquisa de mestrado, combina um modelo digital de afloramento com elementos determinísticos (estratigrafia, caracterização litológica e parâmetros petrofísicos) e redes estocásticas de fraturas carstificadas. Este capítulo tem o intuito de sumarizar o estado da arte dos conceitos menos comuns, a saber DOM (*Digital Outcrop Model*), DFN (*Discrete Fracture Network*) e DFKN (*Discrete Fracture and Karst Network*). Estes conceitos são abordados em duas seções, sendo a primeira sobre os DOMs e a segunda sobre DFNs, a qual também engloba os DFKNs.

2.1 DOM - Modelos Digitais de Afloramento

Uma das etapas fundamentais do processo geocientífico é a investigação *in loco* de afloramentos, os quais são a forma mais direta de obtenção de dados geológicos. Comumente, nesses afloramentos as feições de interesse podem ser observadas, identificadas, medidas, amostradas, entre outros procedimentos. Sob a ótica da geologia do petróleo, as características específicas dos afloramentos, tais como aspectos estruturais, diagenéticos e sedimentológicos, podem servir como exemplos análogos aos processos ocorrentes em escala de reservatório. Por outro lado, há diversas condições que podem inviabilizar uma visita a um afloramento, variando desde limitações orçamentárias até precariedades de acessibilidade e segurança do local.

Os DOMs apresentam-se como um aliado importante dos geocientistas, reproduzindo o campo em um alto grau de detalhamento em um ambiente digital. Conceitualmente, os DOMs referem-se a superfícies 3D (*meshes*) ou nuvens de pontos (Jones et al., 2008) que remontam de forma digital,

por vezes em alta resolução, afloramentos geológicos (Bellian et al., 2005). Os modelos gerados podem ser texturizados a partir de fotografias do afloramento, no caso das superfícies 3D, ou colorizados, no caso das nuvens de pontos (Bistacchi et al., 2022). Hodgetts (2013) destaca ainda que a exploração dos dados em meio digital permite observar o afloramento por pontos de vista antes inacessíveis, aumentando a quantidade de dados adquiridos sem necessariamente aumentar o tempo despendido. Via de regra, os DOMs podem ser construídos a partir de duas ferramentas principais, as quais são o LIDAR (*Light Detection and Ranging*) (Bellian et al., 2005; Furtado et al., 2022; Rotevatn et al., 2009) e a fotogrametria (Nesbit et al., 2020; Triantafyllou et al., 2019).

O LIDAR é o equivalente ótico do radar. Neste método, um feixe laser é disparado contra o objeto de interesse e refletido de volta ao sensor, permitindo o cálculo da distância entre o ponto de reflexão e o equipamento, sabendo-se a velocidade de propagação da luz (Bellian et al., 2005). Ao contrário do LIDAR, a fotogrametria é um método passivo (Remondino & El-Hakim, 2006) que se utiliza de fotografias para recompor o objeto de estudo. Esta técnica lança mão do efeito estereoscópico, no qual a noção de distância é criada pela superposição de imagens cujos ângulos de registro são ligeiramente diferentes (Kuenen, 1950). Com o avanço tecnológico, pares estereoscópicos foram substituídos por extensos conjuntos de fotografias superpostas, as quais registram o objeto de estudo a partir de variados ângulos e posições. Essas fotografias são alinhadas automaticamente por software (Westoby et al., 2012), permitindo então a composição de malhas (*meshes*) e nuvens de pontos.

Trabalhos recentes aplicam o uso de DOMs nos mais variados contextos, envolvendo desde geotecnia (Menegoni et al., 2020) e sedimentologia (Bilmes et al., 2019) até geologia estrutural (Triantafyllou et al., 2019) e espeleologia (Furtado et al., 2022; Pontes et al., 2021). Nestes exemplos, o DOM é utilizado como uma ferramenta para investigar especificidades do objeto ou área de estudo, sendo esse modo de utilização o mais difundido. Seguindo outra lógica, trabalhos a exemplo de Hodgetts et al. (2004); Usman et al. (2021) e Senger et al. (2022), propõem a aplicação integrativa dos DOMs, correlacionando esses modelos digitais a conjuntos de dados complementares de diversas naturezas. O manuscrito "*Integrating stratigraphy, petrophysics and karstified fracture network into a single 3D Digital Model: Example from the Cristal Cave (São Francisco Craton, NE/Brazil)*", contido no corpo desta dissertação e apresentado a seguir, é intrinsecamente

pautado nesses exemplos de abordagem integrativa.

2.2 DFN - Redes de Fraturas Discretas

Os DFNs referem-se a representações computacionais que apresentam, individualmente para cada fratura, parâmetros específicos de orientação, tamanho, posição, forma, abertura e relações topológicas (Lei et al., 2017). A elaboração de um DFN pode se dar por meios estocásticos (Min et al., 2004), determinísticos (Belayneh & Cosgrove, 2004; Zhang & Sanderson, 1996) ou geomecânicos (Renshaw & Pollard, 1994).

Os DFN geomecânicos resultam da solução numérica das equações de propagação do *stress* em um corpo sintético, inicialmente não deformado, a partir de condições de contorno e de *stress* iniciais (Paluszny & Matthäi, 2009; Renshaw & Pollard, 1994).

Por sua vez, os DFNs determinísticos são oriundos de interpretações de dados de campo. Lei et al. (2017) destacam que esses modelos reproduzem bem as características geométricas e topológicas da rede de fraturas observada. Estes autores, no entanto, indicam que essa abordagem não abrange adequadamente problemas 3D com fraturas de mergulho oblíquo, o que decorre da estreita gama de técnicas (GPR, tomografia, etc.) capazes de retornar dados de fato 3D (Jones et al., 2008).

Por fim, os DFNs estocásticos representam as fraturas como formas geométricas simples (elipses, retângulos, etc.) e seguem regras estatísticas para gerar redes de fraturas. Classicamente, esses modelos estimam as dimensões das fraturas seguindo distribuições de lei de potência, gama, lognormal ou exponencial negativa (Bonnet et al., 2001), enquanto que as direções de fratura são estabelecidas a partir de um diagrama de roseta, assumindo uma distribuição estatística normal, uniforme ou de Fisher para cada *set* (Einstein & Baecher, 1982). Alternativamente, o trabalho de Dantas et al. (2022), do qual compartilho a co-autoria, apresenta uma abordagem vinculada inovadora da solução do problema inverso da estereologia, na qual as estatísticas das redes de fraturas medidas nas superfícies expostas do afloramento são utilizadas. Nesse caso, o DFN foi gerado a partir das interpretações estruturais do DOM do Acesso 1 da Caverna Cristal e foi reincorporado no Modelo Integrativo. Este DFN honra os seguintes parâmetros: a) A distribuição estatística dos comprimentos dos traços de fratura mapeados no DOM da caverna, a partir de um histograma

unificado para todas as superfícies (teto e paredes); b) O expoente da lei de potência calculada a partir dos comprimentos dos traços de fratura; c) O parâmetro de persistência P_{21} (Dershowitz & Herda, 1992) dos traços de fratura medidos nas superfícies expostas da caverna e d) O arranjo em conjugação dos *sets* NW-SE e ENE-WSW da Caverna Cristal (La Bruna et al., 2021). Em comparação com Dantas et al. (2022), a única diferença é que o DFN apresentado nesta dissertação é composto por fraturas de forma retangular ao invés de fraturas de formato discóide, aumentando assim similaridade com as fraturas encontradas na natureza.

Em relação aos parâmetros de abertura, os DFNs clássicos levam em conta o valor de abertura mecânica e o coeficiente de rugosidade de cada fratura (Dershowitz & Einstein, 1988). Desse modo, esses DFNs não preveem interações do fraturamento com outros processos, dentre eles o de carstificação, ignorando que as fraturas podem ser alargadas por efeito da dissolução. Nesse sentido, leis de potência modificadas relacionando a abertura de fraturas alargadas por dissolução cárstica ao comprimento de fraturas (Lopes et al., 2021) puderam ser implementadas ao DFN incorporado ao Modelo Integrativo, resultando em diferentes DFKNs. A denominação DFKN é cunhada por Lopes et al. (2021), mas outros trabalhos compartilham do propósito de unir dados de fraturamento e carstificação (Boersma et al., 2019; Fernández-Ibáñez et al., 2019).

Reitera-se, por fim, que os DFNs são ferramentas relevantes e estão em constante desenvolvimento, mas, assim como os DOMs, sua integração com dados complementares ainda é pouco explorada.

Referências Bibliográficas

- Belayneh, M., & J. W. Cosgrove, 2004, Fracture-pattern variations around a major fold and their implications regarding fracture prediction using limited data: an example from the Bristol Channel Basin: Geological Society, London, Special Publications, **231**, 89–102.
- Bellian, J. A., C. Kerans, & D. C. Jennette, 2005, Digital outcrop models: applications of terrestrial scanning lidar technology in stratigraphic modeling: Journal of Sedimentary Research, **75**, 166–176.
- Bilmes, A., L. D'Elia, L. Lopez, S. Richiano, A. Varela, M. del Pilar Alvarez, J. Bucher, I. Eyraud, M. Muravchik, J. Franzese, et al., 2019, Digital outcrop modelling using “structure-from-motion” photogrammetry: Acquisition strategies, validation and interpretations to different sedimentary environments: Journal of South American Earth Sciences, **96**, 102325.
- Bistacchi, A., M. Massironi, & S. Viseur, 2022, 3D Digital Geological Models: From Terrestrial Outcrops to Planetary Surfaces: Wiley.
- Boersma, Q., R. Prabhakaran, F. H. Bezerra, & G. Bertotti, 2019, Linking natural fractures to karst cave development: a case study combining drone imagery, a natural cave network and numerical modelling: Petroleum Geoscience, **25**, 454–469.
- Bonnet, E., O. Bour, N. E. Odling, P. Davy, I. Main, P. Cowie, & B. Berkowitz, 2001, Scaling of fracture systems in geological media: Reviews of Geophysics, **39**, 347–383.
- Dantas, R. R., W. E. Medeiros, & J. V. Pereira, 2022, A constrained version for the stereology inverse problem: Honoring power law and persistences of the fracture traces exposed on arbitrary surfaces: Journal of Petroleum Science and Engineering, **208**, 109661.
- Dershowitz, W., & H. Einstein, 1988, Characterizing rock joint geometry with joint system models: Rock Mechanics and Rock Engineering, **21**, 21–51.
- Dershowitz, W. S., & H. H. Herda, 1992, Interpretation of fracture spacing and intensity: Presented at the The 33rd US Symposium on Rock Mechanics (USRMS), OnePetro.

- Einstein, H. H., & G. B. Baecher, 1982, Probabilistic and Statistical Methods in Engineering Geology I. Problem Statement and Introduction to Solution, booktitle = Ingenieurgeologie und Geomechanik als Grundlagen des Felsbaues / Engineering Geology and Geomechanics as Fundamentals of Rock Engineering: Springer Vienna, 47–61.
- Fernández-Ibáñez, F., P. J. Moore, & G. D. Jones, 2019, Quantitative assessment of karst pore volume in carbonate reservoirs: AAPG Bulletin, **103**, 1111–1131.
- Furtado, C. P., W. E. Medeiros, S. V. Borges, J. A. Lopes, F. H. Bezerra, F. P. Lima-Filho, R. P. Maia, G. Bertotti, A. S. Auler, & W. L. Teixeira, 2022, The influence of subseismic-scale fracture interconnectivity on fluid flow in fracture corridors of the Brejões carbonate karst system, Brazil: Marine and Petroleum Geology, 105689.
- Hodgetts, D., 2013, Laser scanning and digital outcrop geology in the petroleum industry: A review: Marine and Petroleum Geology, **46**, 335–354.
- Hodgetts, D., N. Drinkwater, J. Hodgson, J. Kavanagh, S. Flint, K. Keogh, & J. Howell, 2004, Three-dimensional geological models from outcrop data using digital data collection techniques: an example from the Tanqua Karoo depocentre, South Africa: Geological Society, London, Special Publications, **239**, 57–75.
- Jones, R. R., T. F. Wawrzyniec, N. S. Holliman, K. J. McCaffrey, J. Imber, & R. E. Holdsworth, 2008, Describing the dimensionality of geospatial data in the earth sciences - Recommendations for nomenclature: Geosphere, **4**, 354–359.
- Kuenen, P. H., 1950, Stereoscopic projection for demonstration in geology, geomorphology, and other natural sciences: The Journal of Geology, **58**, 49–54.
- La Bruna, V., F. H. Bezerra, V. H. Souza, R. P. Maia, A. S. Auler, R. E. Araujo, C. L. Cazarin, M. A. Rodrigues, L. C. Vieira, & M. O. Sousa, 2021, High-permeability zones in folded and faulted silicified carbonate rocks – Implications for karstified carbonate reservoirs: Marine and Petroleum Geology, **128**, 105046.
- Lei, Q., J.-P. Latham, & C.-F. Tsang, 2017, The use of discrete fracture networks for modelling coupled geomechanical and hydrological behaviour of fractured rocks: Computers and Geotechnics, **85**, 151–176.
- Lopes, J. A. G., W. E. Medeiros, V. La Bruna, A. Lima, F. H. R. Bezerra, & D. J. Schiozer, 2021,

- Advancements towards DFKN modelling: Incorporating fracture enlargement resulting from karstic dissolution in discrete fracture networks: *Journal of Petroleum Science and Engineering*, **209**, 109944.
- Menegoni, N., D. Giordan, & C. Perotti, 2020, Reliability and uncertainties of the analysis of an unstable rock slope performed on RPAS digital outcrop models: The case of the Gallivaggio landslide (Western Alps, Italy): *Remote Sensing*, **12**, 1635.
- Min, K.-B., L. Jing, & O. Stephansson, 2004, Determining the equivalent permeability tensor for fractured rock masses using a stochastic REV approach: Method and application to the field data from Sellafield, UK: *Hydrogeology Journal*, **12**, 497–510.
- Nesbit, P. R., A. D. Boulding, C. H. Hugenholtz, P. Durkin, & S. Hubbard, 2020, Visualization and sharing of 3D digital outcrop models to promote open science: *GSA Today*, **30**, 4–10.
- Paluszny, A., & S. K. Matthäi, 2009, Numerical modeling of discrete multi-crack growth applied to pattern formation in geological brittle media: *International Journal of Solids and Structures*, **46**, 3383–3397.
- Pontes, C. C., F. H. Bezerra, G. Bertotti, V. La Bruna, P. Audra, J. De Waele, A. S. Auler, F. Balsamo, S. De Hoop, & L. Pisani, 2021, Flow pathways in multiple-direction fold hinges: Implications for fractured and karstified carbonate reservoirs: *Journal of Structural Geology*, **146**, 104324.
- Remondino, F., & S. El-Hakim, 2006, Image-based 3D modelling: a review: *The Photogrammetric Record*, **21**, 269–291.
- Renshaw, C. E., & D. D. Pollard, 1994, Numerical simulation of fracture set formation: A fracture mechanics model consistent with experimental observations: *Journal of Geophysical Research: Solid Earth*, **99**, 9359–9372.
- Rotevatn, A., S. J. Buckley, J. A. Howell, & H. Fossen, 2009, Overlapping faults and their effect on fluid flow in different reservoir types: A LIDAR-based outcrop modeling and flow simulation study: *AAPG Bulletin*, **93**, 407–427.
- Senger, K., P. Betlem, T. Birchall, L. Gonzaga Jr, S.-A. Grundvåg, R. K. Horota, A. Laake, L. Kuckero, A. Mørk, S. Planke, et al., 2022, Digitising Svalbard's Geology: the Festningen Digital Outcrop Model: *First Break*, **40**, 47–55.

- Triantafyllou, A., A. Watlet, S. Le Mouélic, T. Camelbeeck, F. Civet, O. Kaufmann, Y. Quinif, & S. Vandycke, 2019, 3-D digital outcrop model for analysis of brittle deformation and lithological mapping (Lorette cave, Belgium): *Journal of Structural Geology*, **120**, 55–66.
- Usman, M., N. A. Siddiqui, S.-Q. Zhang, M. J. Mathew, Y.-X. Zhang, M. Jamil, X.-L. Liu, & N. Ahmed, 2021, 3D geo-cellular static virtual outcrop model and its implications for reservoir petro-physical characteristics and heterogeneities: *Petroleum Science*, **18**, 1357–1369.
- Westoby, M. J., J. Brasington, N. F. Glasser, M. J. Hambrey, & J. M. Reynolds, 2012, ‘Structure-from-Motion’ photogrammetry: A low-cost, effective tool for geoscience applications: *Geomorphology*, **179**, 300–314.
- Zhang, X., & D. J. Sanderson, 1996, Effects of stress on the two-dimensional permeability tensor of natural fracture networks: *Geophysical Journal International*, **125**, 912–924.

Capítulo 3

Manuscrito Submetido: “*Integrating stratigraphy, petrophysics and karstified fracture network into a single 3D Digital Model: Example from the Cristal (São Francisco Craton, NE/Brazil).*”

Manuscrito PETROL32096 submetido à revista *Journal of Petroleum Science and Engineering* em 08 de Novembro de 2022.

Integrating stratigraphy, petrophysics and karstified fracture network into a single 3D Digital Model: Example from the Cristal Cave (São Francisco Craton, NE/Brazil).

João Victor F. Pereira^a, Walter E. Medeiros^{a,b,g,*}, Renato R.S. Dantas^{b,g}, Francisco H.R. Bezerra^{a,c}, Vincenzo La Bruna^{a,b}, Milton M. Xavier Jr.^{a,b,g}, Rubson P. Maia^d, Daniel D.M. Gomes^e, Danielle C.C. Silva^f, Ingrid B. Maciel^a

^a*Postgraduation Program on Geodynamics and Geophysics, Federal University of Rio Grande do Norte, Natal, Brazil*

^b*Department of Geophysics, Federal University of Rio Grande do Norte, Natal, Brazil*

^c*Department of Geology, Federal University of Rio Grande do Norte, Natal, Brazil*

^d*Department of Geography, Federal University of Ceará , Fortaleza, Brazil*

^e*Department of Geography, University of Pernambuco, Recife, Brazil*

^f*Postgraduation Program on Mineral and Oil Exploration, Federal University of Campina Grande, Campina Grande, Brazil*

^g*INCT-GP/CNPq/CAPES-National Institute of Science and Technology in Petroleum Geophysics/CNPq/CAPES, Brazil*

Abstract

Digital Outcrop Models (DOMs) are visual representations of geological sites in a virtual environment. DOMs are constantly evolving and widely used tools for geological investigations. However, in contrast with their broad applications, the full potential of DOMs is still underexplored in terms of their integration with other data. We present an integrative approach by combining a DOM with stratigraphic, petrophysical, fracture distribution and karst dissolution information into a single 3D georeferenced digital model. Fracture aperture enlargement due to karstic dissolution are implemented on a Discrete Fracture Network (DFN) to generate a Discrete Fracture and Karst Network (DFKN), where it is possible to compose different karstification scenarios. The used DOM is based on photogrammetric data obtained inside the Access 1 of the Cristal Cave. This cave developed in Mesoproterozoic carbonate rocks of the Caboclo Formation, in the Chapada Diamantina Group, São Francisco Craton, Northeastern Brazil, and has been used as a structural and diagenetic outcrop analogue for the Brazilian pre-salt carbonate reservoirs. The described Integrative Model combines both deterministic (stratigraphy and petrophysics) and stochastic (DFN and DFKN) elements. The framework of the Integrative Model reproduces the stratigraphy of the Access 1 as 22 parallel layers, which were populated with measurements of porosity, permeability and uniaxial compressive strength. Resorting to a stochastic approach, we obtained a 3D DFN by solving the stereology inverse problem, where statistical measurements of the fracture traces (power law and P_{21} persistences) on the walls and ceiling of the cave are honored. Petrophysical parameters of the Integrative Model can be easily changed. Also, it is possible to modify the power law that relates aperture and fracture length to implement different karstification stages of the fracture apertures. As a result, different scenarios of primary and secondary porosities can be easily composed, which can be used in fluid flow simulations, thus facilitating the understanding of the multiple

*Corresponding author

Email address: walter.medeiros@ufrn.br (Walter E. Medeiros)

factors affecting the behavior of carbonate reservoirs.

Keywords: Digital Outcrop Model, Discrete Fracture Network, Karst, Carbonate reservoirs.

1. Introduction

The concept of a Digital Outcrop Model (DOM) is well-known in geosciences and refers to virtual representations of outcrops or sites of high geological relevance. These representations are often constructed using laser ranging (Bellian et al., 2005; Buckley et al., 2008) or photogrammetric (James and Robson, 2012) methods, which can be conducted with portable or airborne equipment. Different survey setups result in different coverage areas, spatial resolutions and acquisition speeds. In addition, it is possible to capture colors from the outcrop and generate a photo-realistic texture for the model (Alfarhan et al., 2008; Buckley et al., 2010; Aires et al., 2022).

From an application perspective, DOMs are viable tools in a wide range of geological investigations, due

to the adaptability of the workflows and the relative ease of development. This way, the use of DOMs comprises from geotechnical applications (Menegoni et al., 2020) to structural geology (Triantafyllou et al., 2019; Martinelli et al., 2020), sedimentology (Bilmes et al., 2019) and speleology (Pontes et al., 2021; Furtado et al., 2022) studies. Noticeably, many authors resort to outcrop models as a resource for geological interpretations and measurements. Then, a workflow for developing a DOM must account for many variables for a better fitting between the model and the studied problem. As a consequence, most of the related bibliography is focused in reporting how DOMs are elaborated, usually emphasizing the technical procedures adopted in the workflow (Caravaca et al., 2020; Aires et al., 2022).

Despite being widely used, there is still a need to integrate DOMs with complementary data collected in the field or measured in laboratory. As a consequence, the visualization potential of the 3D environment is

not fully exploited and the ability to correlate complementary data is underutilized. To connect DOMs with other datasets, we present the concept of an Integrative Model (Fig. 1). The proposed 3D Integrative Model takes a georeferenced photogrammetric DOM as a digital basis to embody other available information such as, stratigraphy, petrophysical attributes (e.g. porosity and permeability) and Discrete Fracture and Karst Networks (DFKN) (Lopes et al., 2021) generated by deterministic or stochastic methods.

In particular, we use a DFKN that derives from the combination of two methodologies. The first one refers to a stochastic DFN obtained by solving a constrained stereology inverse problem, as presented in Dantas et al. (2022), where the DFN honors the power law and P_{21} persistences of the fracture traces measured on the walls and ceiling of the cave. The second methodology allows to incorporate enlarged fracture apertures due to karstic dissolution using a modified power law, which correlates fracture apertures to fracture lengths (Lopes et al., 2021).

To exemplify our approach, an Integrative Model is built based on the data from the Cristal Cave, São Francisco Craton, Northeastern Brazil. The Cristal Cave developed in Mesoproterozoic carbonates of the

Caboclo Formation, Chapada Diamantina Group. This environment was chosen because the Cristal Cave is a complex environment presenting fracturing, karstification and silicification processes (Souza et al., 2021; 35 La Bruna et al., 2021), and is therefore considered a structural and diagenetic outcropping analogue for the Brazilian pre-salt carbonate reservoirs. In turn, these reservoirs are responsible for 73% of the whole Brazilian oil production, according to the National Agency for Petroleum, Natural Gas and Biofuels (ANP, 2021).

The features of the Integrative Model and how they are linked are minutely described in Section 3. As presented here, an Integrative Models can be a starting point for the elaboration of static models for fluid flow 40 modeling, for example, which are widely used in the oil industry. In spite of the small scale of the example, the methodology is meant to be reproducible in large scale problems, which fits for oil industry applications.

2. Geological Setting

The chosen example to support our methodology is the Cristal Cave, a karstic system located in the eastern side of the São Francisco Craton, central-eastern Chapada Diamantina Basin (Fig. 2). This cave 45 is 6.7 km long in total (Fig. 3a) and it was developed in the rocks of the Caboclo Formation, Chapada Diamantina Group (Fig. 4). The geological context of the Cristal Cave is complex and presents a diverse range of geological processes, including fracturing, silicification and karstic dissolution events. This abundance of processes was the reason to take this cave as an example for the construction of an Integrative Model and, in this sense, a brief description of the cave geological context is necessary

50 2.1. Regional tectonic contextualization

The basement of the rocks related to the Cristal Cave is the Gavião Block, which is one of the constituting Archean blocks of the São Francisco Craton (Barbosa and Sabaté, 2002). This block is mainly composed of Archean orthogneiss complexes, including TTG (Tonalite-trondhjemite-granodiorite) assemblages, and they are associated to volcano-sedimentary units (Barbosa and Sabaté, 2004). The crustal recycling during the 55 Transamazonian Orogeny (2.02.1 Ga) induced the development of greenstone belts and the migmatization of the TTG units (Pinto et al., 1998).

Accordingly to Alkmim and Martins-Neto (2012), the São Francisco Craton, including the Gavião Block, was submitted to, at least, two major rifting events in between 1.75 and 1.65 Ga. These events generated a late Paleoproterozoic to Mesoproterozoic rift-sag system, inducing the deposition of the Espinhaço 60 Supergroup. Considering the Chapada Diamantina region, this Supergroup comprises the groups Rio dos Remédios, Paraguaçú, Chapada Diamantina and Una (Fig. 4).

2.2. Stratigraphy of the Chapada Diamantina region

The Rio dos Remédios Group presents siliciclastic rocks of lacustrine to alluvial origin, volcanic rocks of acid composition and tuff deposits (Heilbron et al., 2016). The detrital zircons, analyzed by Guadagnin et al.

65 (2015) for those rocks, date from 1.8 to 1.68 Ga, which is consistent with the first rifting event proposed by Alkmim and Martins-Neto (2012).

According to Heilbron et al. (2016), the Paraguaçú Group consists of sandstones, pelites and mafic volcanic intrusions deposited in a graben setting, by fluvial, eolian and marine systems. U-Pb ages from Guadagnin et al. (2015) correlates the evolution of the Paraguaçú Group to a second rifting episode, endorsing the second 70 rifting phase proposed by Alkmim and Martins-Neto (2012).

The Chapada Diamantina Group is the youngest and most prominent unit of the Espinhaço Supergroup. This group is subdivided in three formations, which are Tombador, Caboclo and Morro do Chapéu (base to top). Magalhães et al. (2014) describe the Tombador Formation as an evolution of a braided-fluvial system to a shallow-marine system, also involving sheet floods, floodplains and estuarine deposits, roughly resulting 75 in several sandstone facies. Zircons from tuffs deposited in the upper section of the Tombador Formation present U-Pb ages of 1436 ± 26 Ma (Guadagnin et al., 2015). This age correlates the Tombador Formation deposition to the second rifting phase. The Caboclo Formation lithologies were deposited in a mixed carbonate-siliciclastic ramp in a shallow-marine environment, strongly influenced by storm waves (Ferronatto et al., 2021). In this context, the storm waves induced the deposition of conglomerate and sandstone facies, 80 while also generated erosive surfaces. Thus, the accretion of the stromatolite units (Srivastava and Rocha, 2002) occurs under fair-weather periods (Ferronatto et al., 2021). The Pb-Pb age of the stromatolite units is 1140 ± 140 Ma (Babinski et al., 1993).

The Cristal Cave developed in the carbonate facies of the Caboclo Formation. In the cave itself, Souza et al. (2021) detailed six different lithofacies, which are: ooidal grainstones, intraclastic grainstones and 85 rudstones, heterolites, marls, stromatolites, oncolithic-intraclastic grainstones, as well as rudstones, and fault-related hydraulic breccias. These lithofacies present different porosities and silica content, thus affecting permeability and karst development (Souza et al., 2021; Ferronatto et al., 2021). Furthermore, the marl layers are considered as a top seal for the cave, which inhibits karstification in the upward direction (Souza et al., 2021). Similar lithological controls over the karstified levels are observed in other caves of Chapada 90 Diamantina and Irecê basins (Ennes-Silva et al., 2016; Cazarin et al., 2019; Pontes et al., 2021).

The Morro do Chapéu Formation is essentially a siliciclastic unit, composed of basal conglomerates, sandstones and minor occurrences of siltstones and mudstones. These rocks were deposited in alluvial braidplains grading to shallow marine conditions (Souza et al., 2019).

The Una Group overlies the Chapada Diamantina Group, and involves the Bebedouro and Salitre Formations. The Una Group presents a vast registry of glaciation episodes. In the Bebedouro Formation, 95 Guimaraes et al. (2011) describe diamictites, sandstones and pelites, deposited in a glacial-marine environment. Otherwise, in the Salitre Formation, Misi and Veizer (1998) identify dolomites, limestones, dolostones, shales and oolithic limestones. The maximum depositional ages are 874 ± 9 Ma for the Bebedouro Formation (Figueiredo et al., 2009) and 670 Ma for the Salitre Formation (Santana et al., 2021).

100 *2.3. Insertion of the Crystal Cave in the regional tectonic context*

The rocks of the Una and Chapada Diamantina groups are juxtaposed by several directional reverse faults (Fig. 2) of NE-SW direction, which mark the limits of Irecê and Chapada Diamantina basins. The referred regional structures can be traced in elevation maps, distinguishing the contiguous basins (Fig. 5). The directional faults are related to the far field stress imposed by the Riacho do Pontal Mobile Belt over the São Francisco Craton during the Brasiliano Orogeny, resulting in a thin-skin deformation of the Proterozoic coverage (Caxito and Uhlein, 2013). Oliveira and Medeiros (2018) present that the northern São Francisco Craton crustal block is rooted underneath the Riacho do Pontal Mobile Belt, emphasizing the thin-skin deformation hypothesis. The stress field imposed by the Riacho do Pontal southward motion originated the thrust-and-fold belt in the Irecê Basin and gentle N-S to NNW-SSE folds in the Chapada Diamantina Basin (Süssenberger et al., 2014).

The abundance of structures has favored the development of several karstic systems, which are not chronologically related to the Cristal Cave, but share a genetic history strongly related to structural control. This way, it is noticeable the association of these caves to hinge zones of fault-propagation folds, as in Toca da Boa Vista and Toca da Barriguda caves (Ennes-Silva et al., 2016; Cazarin et al., 2019), or hinges of basin-dome folded zones, as in Ioi, Lapinha, Paixão and Torrinha caves (Pontes et al., 2021). The cited caves occur in the Neoproterozoic basins of Irecê and Una-Utinga and the related folds occur due to flexural-slip mechanisms, which trigger concomitant fracturing processes (Fig. 6).

Locally at the Cristal Cave, the folded structures are positioned in the shortening quadrant of the major directional reverse fault, resulting in a sequence of open to gentle anticlines and synclines of NNE direction. In turn, the fold morphologies control the Cristal Cave maze (Fig. 3). La Bruna et al. (2021) point out that the main conduit orientations, as shown in Figure 3A, coincide with the axes of regional scale folds. Besides that, fractures tend to concentrate along the fold hinges or align with major normal faults, developed in the extensional quadrant of the main reverse fault (La Bruna et al., 2021).

3. Methodology

The main challenge we faced in the elaboration of the Integrative Model was to combine datasets from both digital and analogical sources in a 3D georeferenced environment. Our starting datasets were a photogrammetric DOM, fracture interpretations from the DOM, a lithological column constructed in the field, petrophysical measurements on field-collected samples and a stochastically generated Discrete Fracture Network (DFN). The next subsections report not only how we obtained each one of these datasets, but also how we managed to interconnect them into a single Integrative Model.

3.1. Photogrammetric Model

We used a photogrammetric DOM resulting from high resolution photos taken inside the Access 1 of the Cristal Cave (Fig. 3), which were aligned to compose a polygonal mesh model. This mesh model represents

the cave geometry as triangulated surfaces, which can be combined with a texture layer, constructed from the
135 original photographs. Control points could be imaged outside the cave, allowing the model to be georeferenced in its X (N), Y (E) and Z (depth) dimensions. The resulting model has 3.66 million faces and its texture has a 16 megapixel resolution. We used the CloudCompare software (Girardeau-Montaut, 2022) to visualize the DOM and the Compass plugin (Thiele et al., 2017) to interpret the fracture network. The generation and visualization of complementary datasets also occurred in the CloudCompare environment.

140 *3.2. Fracture interpretation from the DOM*

The resulting spatial resolution of the model was enough to interpret medium sized to large sized fractures occurring in the Access 1. The fractures are present in the walls and ceiling of the cave, where they can be exposed in multiple surfaces simultaneously, or they can cut only one surface. This variation of exposition surfaces required different interpretation approaches. For organization purposes, we grouped these fractures
145 in two subsets, named as Group A and Group B.

As shown in Figure 7, Group A contains fracture traces that intercept multiple surfaces simultaneously (one wall and the ceiling, for example). In this case, the interpreted traces can be used to obtain a fracture plane of well-defined dimensions and attitudes. On the other hand, Group B contains fracture traces that intercept only one surface (only the ceiling, for example). Whenever fracture traces of Group B are nearly
150 horizontal, it is possible to determine the fracture plane strike but the dip value is not available.

3.3. Fieldwork

Fieldwork was focused in three objectives. The first one was to ascertain the limits of the photogrammetric data regarding the structural interpretation. To validate the virtually acquired structural parameters, we compared the obtained attitudes with *in situ* measurements taken with a geological compass. Concerning
155 fracture directions, the two datasets present no significant differences. However, we detected in the field abundant stratabound fractures of small scale, as compared with the virtually mapped fractures (Fig. 8). From this comparison, we decided that fracture scales obtained from the DOM interpretation, which approximately range from 2 m to 60 m, are sufficient to build a DFN to be used in fluid flow simulations.

The second objective of the fieldwork was to characterize a lithological section for the Access 1, as we
160 concluded that it was not possible to reliably identify lithologies using only the DOM, even taking into account the texture and color attributes. This limitation is related to the conjunction of poor lighting conditions (compared to the sunlight) and the frequent weathered/mossy aspect of the rock surfaces inside the cave. The identified lithological section is shown in Figure 9 and encompasses the *in loco* macroscopic description of each layer and the identification of visual reference points (also shown in Fig. 9), which were
165 used to tie the lithological section to the DOM. For the layer descriptions, we took advantage of the horizontal continuity of the layers and the topographical variations inside and outside the cave to also incorporate the lithological units located above the cave ceiling. For each lithology, we measured the uniaxial compressive strength (UCS) *in situ* and sampled a rock plug for further petrophysical laboratory measurements, to be

later detailed. Note that all petrophysical measurements are tied to the lithological section and, consequently,
170 to the DOM.

For the third and final objective, we visited specific areas of the Access 1 that were poorly reproduced in
the DOM to investigate the real condition of the outcrop and the potential causes of the bad imaging (low
light conditions, complex outcrop geometry and so forth). This procedure aimed to better understand the
limits of the DOM in order to mitigate uncertainties from the virtual interpretation.

175 *3.4. Petrophysics*

We collected a sample for each layer mapped in the lithological section, resulting in 22 cylindrical plugs.
Among them, we selected 18 plugs that matched the minimum specifications of size and integrity for petro-
physical measurements, which were done with the Coreval 700 unsteady state gas permeameter and porosimeter
(Vinci Technologies, France).

180 In the field, we measured the uniaxial compressive strength (UCS) for each layer, just before the plug
extraction or at a safe distance (15 to 20 cm) from the plug holes. This choice aimed to keep the data
correlation while avoiding the mechanical disturbed zone caused by the drilling process. UCS measurements
were done with a portable Schmidt hammer (Proceq™) and every presented UCS estimate is the arithmetic
mean of 10 measurements taken in a circular sampling area of 5 cm diameter. UCS measurements were made
185 mainly in the horizontal direction due to the predominance of subvertical exposition surfaces. However,
whenever it was possible, we also took measurements in the vertical direction. In both cases, the Schmidt
hammer was kept perpendicular to the target surface. Obtained measurements are shown in Figure 9.

190 *3.5. 3D DFN and DFKN generation*

The fracture mapping from the DOM supported the generation of a stochastic Discrete Fracture Network
model (DFN), which reproduces some observed statistics of the fracture sets. The constrained DFN building
is based on the solution of the inverse problem of stereology, as described in Dantas et al. (2022). Below, we
summarize the key points of the DFN generation, where a solution of the inverse problem of stereology is
obtained honoring:

- 195 • The statistical distribution of the fracture lengths exposed in the cave surfaces, named as fracture
traces. A single fracture trace frequency histogram was obtained for all exposed surfaces.
- The power law exponent for the observed length of the fracture traces.
- The P_{21} persistence parameter of the fracture traces measured on the exposed surfaces of the cave. P_{21}
refers to the total fracture length per unit area in a sampled surface (Dershowitz and Herda, 1992).
- 200 • The conjugate arrangement of the NW-SE and ENE-WSW sets, which is admitted to be valid for the
characterized fracture sets (La Bruna et al., 2021).

In relation to the methodological approach presented in Dantas et al. (2022), only one modification was done: here, instead of using a disk shape for the fractures, we represented all fractures as rectangular planes of constant thicknesses and with a length/height aspect ratio of 2:1. As solution of the inverse problem of stereology we obtain a P_{32} estimate (Dershowitz and Herda, 1992) for a prismatic volume, equivalent to approximately eight times the volume of the Access 1. Then, a particular DFN is stochastically generated.

Finally, different scenarios of fracture aperture distributions for the obtained DFN are generated taking into account the enlargement of the fracture apertures due to karstic dissolution, resulting in DFKN models. This way, different karstic dissolution stages of the fracture network can be implemented. The key point of this methodology is that karstic dissolution progressively destroys the linear dependence (in log \times log plots) between fracture aperture and fracture length, which is typical of mechanically originated fractures, as explained in Lopes et al. (2021).

4. Results

4.1. Incorporating stratigraphy and petrophysics in the Integrative Model

We combined the DOM and the lithological section to generate a 3D stratigraphic model, by assigning thickness and depth to each layer (Fig. 9). The lithological section was then used as a pseudo-well, allowing to tie the stratigraphic section to the photogrammetric data.

It was possible to detect subtle differences in the dip direction values for the layers of the Access 1. Measurements from the DOM (Fig. 10) indicate an approximate dip value of 3° for the bedding. However, on the east wall the bedding dips to east, while on the west wall the bedding dips to west. This behavior indicates the existence of an anticline in the Access 1, where the anticline axis is coincident with the main corridor of the access. This result is concordant with the occurrence of folds in the Chapada Diamantina locality, well documented in regional scale geologic maps (Menezes et al., 2019), and detailed descriptions of the corridors of the Cristal Cave (La Bruna et al., 2021). Due to the fact that the folding is very gentle, for simplicity we reproduce the strata in the Integrative Model as nearly horizontal layers of constant thickness with a vertical stacking pattern. The resulting layer cake model is centered on Access 1 of the cave (Fig. 11A), but its volume is approximately eight times the volume of Access 1. The obtained rectangular prism is used to accommodate the stochastic DFN to be incorporated (see section 4.4).

We use the 3D stratigraphic model as the main geometric feature for composing the Integrative Model. The geometry of the modeled strata can be populated with any additional data, such as lithological information or petrophysical measurements, resulting in different attribute cubes (Fig. 11).

4.2. Evaluation of petrophysical results

Based on Figure 11, it is possible to distinguish two sectors of slightly different petrophysical signatures: one from the top to the middle of the attribute cubes and the other at the bottom of the cubes. To investigate the correlation between different petrophysical parameters, we cross-plotted the values of attribute pairs and marked the respective sector of each sample (Fig. 12).

4.2.1. Porosity and Permeability

The acquired datasets are mainly composed of low values of porosity and permeability, with porosity values ranging from 1.13 to 3.13% and permeability values ranging from 0.0018 to 0.0054 mD. At first sight, these results cannot be directly correlated to lithologic variations, since similar lithologies can present distinct
240 porosity and permeability values (see intraclastic grainstones at 3 m and 7 m, Figure 9). However, accordingly to Figure 12, porosity and permeability values present a reasonable linear correlation although they are not strictly controlled by the depth of the samples.

Taking into account that the silicification process is abundant in the Crystal Cave (Souza et al., 2021), it is possible to speculate that this process has flattened porosity and permeability values for the whole
245 lithological column. However, samples from different sectors of the column show similar correlations between porosity and permeability, suggesting that the local vertical span of the silicification process is not controlled exclusively by stratigraphy. Additionally, we found that rock samples that do not fit the linear correlation between porosity and permeability often present structural discontinuities, such as fractures and stylolites, which affect both porosity and permeability.

250 4.2.2. Uniaxial Compressive Strength

The obtained vertical profiles of the mean uniaxial compressive strength are shown in Figure 9. It is noticeable the high variance of the UCS measurements throughout the column, a result from the fact that the equipment is sensitive to minor changes on the rock surface and to the presence of structural discontinuities. Thus, instead of focusing on absolute values, we prefer to highlight trends and patterns along the column to
255 support our interpretation.

Comparing horizontal and vertical UCS measurements (Fig. 12B), it is clear that the variance effect disturbs the correlation between the samples, but not deeply enough to nullify it. Additionally, there is a persistent association of the upper levels (Fig. 12B, markers in warm colors) of the column with higher values of UCS, while lower levels (Fig. 12B, markers in blue color) present lower UCS values. In the Figures 11E
260 and F, it is possible to distinguish a so-called weaker package related to the basal units of the Access 1. These units coincide with the most karstified levels of the Access 1.

4.3. Fracture interpretation from the DOM

The fracture interpretation workflow is based on the following main criteria: Fractures undoubtedly observable in two or more faces of the model (walls and roof, for example) were discretized as planes and clustered
265 in Group A. Otherwise, fractures observed in only one surface (only in the roof, for example) were mapped as lines and clustered in Group B. For the Access 1 (Fig. 13), 10 fractures were identified in Group A and 24 in Group B. Analysing this dataset, it was possible to separate three main fracture sets, oriented in the NE-SW, ENE-WSW and NW-SE trends. The final result of the virtual fracture interpretation is shown in Figure 7. The NE-SW set is parallel to the trend of the Access 1 corridor and presents the largest fracture lengths. On the other hand, the ENE-WSW and NW-SE sets are mainly composed of smaller but more
270

frequent fractures. In accordance with La Bruna et al. (2021), ENE-WSW and NW-SE sets are interpreted as a conjugated pair of fractures.

It is noticeable that the orientation of these sets strongly coincide with the directions of the major structures, such as the regional scale normal faults (Figs. 2 and 5). Beyond that, the fold hinge trend in the Access 1 and the fracture sets orientations present a good correlation with the model presented in the Figure 6, where the NE-SW set is parallel to the fold hinge and roughly bisects the conjugate sets.

Similarly to the beddings, the major fractures described in the Access 1 present dissolution features along the fracture planes, thus enlarging the fracture aperture values (Fig. 14A). This dissolution process can be interpreted as a result of fluid circulation, indicating that the fractures acted as the preferable pathway for the fluids. Commonly, these fractures are not limited by specific strata and cuts through the cave height. However, we do not discard the hypothesis of a larger scale stratigraphic control over those structures (bed packages or bed package associations).

On the other hand, the smallest fractures detectable in the Access 1 are sub-vertical stratabound discontinuities of decimetric scale (Figs. 14B and 14C). These small structures are horizontally and vertically dispersed along the beds and, predominantly, do not present prominent dissolution.

4.4. Incorporating the DFN in the Integrative Model

After solving the stereology inverse problem using the constrained approach of Dantas et al. (2022), a DFN that honors all statistics of the fractures measured in the Acess 1 was stochastically generated. Thus, the obtained DFN statistically reproduces the occurrence of the NW, NNE and ENE fracture sets, where the NNE and ENE sets are considered a conjugate pair. It is worthwhile to mention that the estimated P_{32} persistences are equal to 0.111, 0.105, and 0.107 to the NW, NNE and ENE fracture sets, respectively. In addition, the estimated exponent values for the power laws governing the statistical occurrence of fracture lengths are equal to 2.59, 2.53, and 2.57 to the NW, NNE and ENE fracture sets, respectively. The resulting DFN is shown in Figure 15A and is composed by 272 fracture planes of rectangular shape. Note that the DFN is contained in the volume assigned to the Integrative Model (Fig. 11)

To allow a visual evaluation of the fracture sets reproduction, Figures 15B-D show the fracture traces resulting from the intersection of the DFN with simplified versions of the exposed surfaces of the cave in Access 1. Note that although individual fracture traces are not reproduced, P_{21} persistences are quite well reproduced in all surfaces. Thus, from an engineering perspective, the DFN is a usable representation of nature because it resulted in a consistent reproduction of the mapped fracture network in terms of strike, dip and fracture density.

4.5. Incorporating fracture enlargement due to karstic dissolution in the Integrative Model

The presented DFN is a first approach to statistically represent a natural fracture network. While it accomplishes the objective of representing the fracture planes in a 3D environment, the DFN does not include aperture variations in the resulting network. In contrast, the fractures observed in the field present different

levels of aperture enlargement, which are strongly affected by karstic dissolution processes. Then, following Lopes et al. (2021), fracture enlargement due to karstic dissolution was incorporated in the Integrative Model based on a progressive modification of the power law relating fracture length and aperture. Specifically, karstic dissolution progressively destroys the linear dependence (on log × log plots) of aperture with length,
310 starting from the largest apertures (Lopes et al., 2021). Figure 16A shows four stages (I to IV) of karstic dissolution that we implemented for the DFN. In this figure, each line is a step-wise approximation of a power law (stage I) that is progressively destroyed, such that, in the last stage of karstic dissolution (IV), fracture apertures show the same value, regardless of fracture length.

We assume that the four shown stages (Fig. 16A) compose a gross representation of the karstic dissolution
315 process in Access 1, where very large fractures actually present apertures close to 0.3 m. Figures 16C-D show the intersections of the resulting DFKNs with the horizontal and E-W vertical planes, respectively, which pass close to the center of the Integrative Model. In addition, Figure 16B shows the associated progressive evolution of the karstified fracture porosity. Note that high values of secondary porosity might be obtained.
320 This kind of evolutive scenarios could be of value, for example, for an engineer that is trying to evaluate if the dual-porosity model (Warren and Root, 1963) is still valid for a karstified fracture network.

5. Discussion

5.1. Innovative aspects of Integrative Models

In spite of the wide utilization of DOMs for geoscientific applications, there is still a predominance in its use as an isolated tool for visualization and interpretation of specific subjects. Throughout the bibliography,
325 only a few papers present methodologies centered in DOMs and data integration, being Hodgetts et al. (2004), Usman et al. (2021) and Senger et al. (2022) good examples of this approach. Hodgetts et al. (2004) and Usman et al. (2021) present similar industry-driven approaches, resorting to commercial softwares (VRGSTM and PetrelTM) to interpret, integrate and derive models from industry standard data types in oilfield-scale problems. In turn, Senger et al. (2022) focus on the use of DOMs and complementary geological
330 data for educational purposes, under the guidelines of the Svalbox open database project (Senger et al., 2021).

Our Integrative Model is a oriented approach to better handling geological data in a fluid flow modeling environment, trying to bridge the gap between the viewpoints of geophysicists/geologists and engineers. Specifically, we achieved a reduction in the methodological gap between the raw geological data from outcrop
335 analogues and a workable model that is closer to the static models used by reservoir engineers. The particular example of Integrative Model explored a small scale case with limited data availability and an increased level of complexity due to the superposed geological processes. In this regard, the Integrative Model was able to incorporate tailor-made solutions, such as the DFN and DFKN models, which were essential to statistically and visually assess the fracture and dissolution patterns in the Cristal Cave. This way, the proven importance

340 of our work is centered in the developed methodology, which encompass the relevance of the Cristal Cave example but not being limited to it.

5.2. The Integrative Model as a tool to karst investigation

The Integrative Model may be used to shed light on the factors affecting karst processes in the Cristal Cave. The petrophysical data shows a vertical compartmentalization of the cave in two overlapped sectors. 345 The lower one is located just below the middlemost heterolite layers and it concentrates the lowest values of permeability and UCS measurements (both vertical and horizontal), while the porosity is relatively low but not significantly. In turn, the upper sector concentrates the highest values for each one of the measured parameters (porosity, permeability and UCS).

The lower section mainly coincides with the alternation of ooidal grainstones with the oncolithic-intraclastic 350 grainstones and rudstones unit. This alternation is a notable controlling factor of the horizontal dissolution along the layers, directly affecting the relief of the walls. For the upper section, this effect is diminished and the internal shape of the corridors gets narrower towards the marl unit, resulting in a domed termination. In this regard, these results corroborate the hypothesis of a stratigraphic control over the karst evolution, which 355 conditioned the propagation of the dissolution to levels below the marl layer. The sealing behavior of the marl unit could not be outlined by the petrophysical measurements, because its porosity and permeability values are not noticeably different from other lithologies (Fig. 9). Possibly, the petrophysical behavior of the layers was homogenized by the silicification process. These observations reiterate the key role of the integrative approach in investigating the geological processes in such a complex environment.

As a general controlling factor, the large scale fractures interpreted from the DOM showed that the general 360 morphology of halls and conduits of the cave are strongly influenced by the fracture parameters. The cave corridors are horizontally aligned to major fracture trends, while the vertical amplitude of the corridors are correlated to the fracture heights. These fractures are statistically represented in the DFKN, without any kind of direct reproduction of positional parameters.

5.3. Karst behavior prediction from DFKN models

365 The stochastically generated DFN have no explicit control on fracture positioning and, as consequence, on the derived DFKNs. Nonetheless, the generated DFN trusty replicates the statistical parameters of the mapped fracture sets. As mentioned, these fractures impose a relevant morphological control on the karstic features of the Cristal Cave. However, both field measurements of fracture apertures and generated DFKNs do not show fractures wide enough to account for the development of the horizontal dimensions of 370 the cave corridors. We interpret this discrepancy as a clue that the cave corridors possibly result from the dissolution of aligned bundles of fractures instead of a single fracture. In case this hypothesis is true, maps of P_{21} persistence could be used to predict where possible corridors would develop inside the generated DFN. Figure 17 support this hypothesis. Note that, based on P_{21} density maps from the DFN, it was possible to

delimit highly fractured zones that present similar shapes either to the Access 1 itself (Figs. 17A, C, and D) 375 and to the cave corridors appearance (Figs. 17B, E, and F) .

5.4. Challenges in the use of DOMs

Undoubtedly, Digital Outcrop Models are a fundamental tool for modern geological investigations, where the possibility to visualize, interpret and integrate outcrop data in the office is an extremely valuable resource. Furthermore, it is relevant to mention that this research was conducted mainly during the social distancing 380 period, due to the COVID pandemic scenario, and the use of DOMs allowed the continuity of the activities away from the field. This eventful context potentialized the value of this tool but it is still essential to clearly state the challenges and limitations of this technique.

Notably, the DOM of the Access 1 was carefully built and it has high standards for spacial resolution and texture quality. However, the imaged site presents an intricate combination of adverse factors, such as 385 accessibility limitations, low lighting conditions, and disturbed outcrop colors due to weathering processes. These factors inhibited any reliable virtual interpretation regarding lithology and stratigraphy. In this context, the interpretation of small scale fractures (less than 2 m) is also compromised. Thus, it is evident that the DOMs, as isolated tools, can not replace the field experience in any aspect. However, it is possible to access the full potential of DOMs by adding field validation steps in the workflow and integrating these 390 models with complementary datasets, aligned with the objectives of the investigation. Thus, we reiterate the importance of an integrative focus in the use of DOMs, as approached in our methodology.

6. Conclusions

The presented concept of Integrative Model is centered in how DOMs can be combined with other datasets. For this work, we took the Cristal Cave as an example, where the Access 1 photogrammetric DOM was 395 combined with stratigraphic and petrophysical data. In addition, the Discrete Fracture Network (DFN) generation supported the implementation of fracture apertures enlarged by karstic dissolution to generate Discrete Fracture and Karst Networks (DFKNs). Through this implementation, fracture apertures were changed to compose different karstification scenarios. The Cristal Cave example was carefully chosen, since it is an outcrop analogue for the Brazilian pre-salt carbonate reservoirs, having in common the occurrence of 400 fracturing, dissolution and silicification processes.

In particular, our approach intended to better align the scopes of geophysicists/geologists and reservoir engineers. In this sense, we resorted to DOMs and digital environments as data handling facilitators, as well as integration tools. This way, we achieved a shorter path between the raw geological data from outcrop analogues and a functional model, closer to the static models used in fluid flow modeling by engineers.

405 Despite the relevance of the chosen example, this research has a strong methodologic driven approach and aimed to develop a workflow to be used in problems of variable scales, which includes oil industry applications. We then reiterate that implementations such as the DFN and DFKN are not exclusive for the

chosen example of the Cristal Cave. These models are actually working tools which can be adapted for the specific parameters of any application case and compounds the core of the presented Integrative Model.

410 **Acknowledgements**

This work is part of the CristalDOM project, a collaboration between Petrobras and the Federal University of Rio Grande do Norte, coordinated by Prof. Hilrio Bezerra (UFRN) and Dr. Delano Menecucci (Petrobras). CristalDOM project is thanked for the MSc scholarship to JVFP. The Brazilian agency CNPq is thanked for the research fellowships and associated grants to WEM and FHRB. The Laboratory of Petroleum Reservoirs 415 Engineering (LABRES/UFRN) is acknowledged for the promptness in executing the petrophysical analyses. Ulson Campos (CECAV - ICMBio) and Augusto Auler (Instituto do Carste) are thanked for the guidance and safety procedures during the fieldwork. Dra. Juliana Lopes is personally thanked for the enriching discussions along the course of this research. The financial support to purchase the computational infrastructure used in this study was given by the INCT-GP (CNPq /CAPES).

420 **References**

- Aires, A.S., Marques Junior, A., Zanotta, D.C., Spigolon, A.L.D., Veronez, M.R., Gonzaga Jr, L., 2022. Digital outcrop model generation from hybrid uav and panoramic imaging systems. *Remote Sensing* 14, 3994. URL: <https://doi.org/10.3390/rs14163994>, doi:10.3390/rs14163994.
- Alfarhan, M., White, L., Tuck, D., Aiken, C., 2008. Laser rangefinders and arcgis combined with three-dimensional photorealistic modeling for mapping outcrops in the slick hills, oklahoma. *Geosphere* 4, 576–587. URL: <https://doi.org/10.1130/GES00130.1>, doi:10.1130/GES00130.1.
- Alkmim, F.F., Martins-Neto, M.A., 2012. Proterozoic first-order sedimentary sequences of the São Francisco Craton, eastern Brazil. *Marine and Petroleum Geology* 33, 127–139. URL: <https://doi.org/10.1016/j.marpetgeo.2011.08.011>, doi:10.1016/j.marpetgeo.2011.08.011.
- ANP, 2021. Boletim da Produo de Petrleo e Gs Natural. Technical Report 127. Brazilian National Agency for Petroleum, Natural Gas and Biofuels.
- Babinski, M., Van Schmus, W., Chemale Jr, F., Brito Neves, B.d., Rocha, A., 1993. Idade isocrônica Pb/Pb em rochas carbonáticas da Formação Caboclo em Morro do Chapéu, BA. Simpósio sobre o Cráton do São Francisco 2, 160–163.
- Barbosa, J.S., Sabaté, P., 2002. Geological features and the Paleoproterozoic collision of four Archean crustal segments of the São Francisco Craton, Bahia, Brazil: a synthesis. *Anais da Academia Brasileira de Ciências* 74, 343–359. URL: <https://doi.org/10.1590/S0001-37652002000200009>, doi:10.1590/S0001-37652002000200009.
- Barbosa, J.S.F., Sabaté, P., 2004. Archean and Paleoproterozoic crust of the São Francisco craton, Bahia, Brazil: geodynamic features. *Precambrian Research* 133, 1–27. URL: <https://doi.org/10.1016/j.precamres.2004.03.001>, doi:10.1016/j.precamres.2004.03.001.
- Bellian, J.A., Kerans, C., Jennette, D.C., 2005. Digital outcrop models: applications of terrestrial scanning lidar technology in stratigraphic modeling. *Journal of sedimentary research* 75, 166–176. URL: <https://doi.org/10.2110/jsr.2005.013>, doi:10.2110/jsr.2005.013.
- Berbert-Born, M.L.C., Rocha, A.J.D., 1995. Espeleologia, in: Rocha, A.J.D., Costa, I.V.G. (Eds.), Projeto Mapas Municipais - Município de Morro do Chapéu. Serviço Geológico do Brasil, Salvador(BA). chapter 15, pp. 158–192.
- Bilmes, A., D'Elia, L., Lopez, L., Richiano, S., Varela, A., del Pilar Alvarez, M., Bucher, J., Eymard, I., Murvachik, M., Franzese, J., et al., 2019. Digital outcrop modelling using structure-from-motion photogrammetry: Acquisition strategies, validation and interpretations to different sedimentary environments. *Journal of South American Earth Sciences* 96, 102325. URL: <https://doi.org/10.1016/j.jsames.2019.102325>, doi:10.1016/j.jsames.2019.102325.

- Buckley, S.J., Howell, J., Enge, H., Kurz, T., 2008. Terrestrial laser scanning in geology: data acquisition, processing and accuracy considerations. *Journal of the Geological Society* 165, 625–638. URL: <https://doi.org/10.1144/0016-76492007-100>.
455
- Buckley, S.J., Schwarz, E., Terlaky, V., Howell, J.A., et al., 2010. Combining aerial photogrammetry and terrestrial lidar for reservoir analog modeling. *Photogrammetric Engineering & Remote Sensing* 76, 953–963. URL: dx.doi.org/10.14358/PERS.76.8.953, doi:10.14358/PERS.76.8.953.
- Caravaca, G., Le Mouélic, S., Mangold, N., LHaridon, J., Le Deit, L., Massé, M., 2020. 3d digital outcrop model reconstruction of the kimberley outcrop (gale crater, mars) and its integration into virtual reality for simulated geological analysis. *Planetary and Space Science* 182, 104808. URL: <https://doi.org/10.1016/j.pss.2019.104808>, doi:10.1016/j.pss.2019.104808.
460
- Caxito, F.d.A., Uhlein, A., 2013. Arcabouço tectônico e estratigráfico da Faixa Riacho do Pontal, Divisa Pernambuco-Piauí-Bahia. *Revista Geonomos* 21. URL: <https://doi.org/10.18285/geonomos.v21i2.269>, doi:10.18285/geonomos.v21i2.269.
465
- Cazarin, C.L., Bezerra, F.H., Borghi, L., Santos, R.V., Favoreto, J., Brod, J.A., Auler, A.S., Srivastava, N.K., 2019. The conduit-seal system of hypogene karst in Neoproterozoic carbonates in northeastern Brazil. *Marine and Petroleum Geology* 101, 90–107. URL: <https://linkinghub.elsevier.com/retrieve/pii/S0264817218305245>, doi:10.1016/j.marpetgeo.2018.11.046.
- Dantas, R.R., Medeiros, W.E., Pereira, J.V., 2022. A constrained version for the stereology inverse problem: Honoring power law and persistences of the fracture traces exposed on arbitrary surfaces. *Journal of Petroleum Science and Engineering* 208, 109661. URL: <https://doi.org/10.1016/j.petrol.2021.109661>, doi:10.1016/j.petrol.2021.109661.
470
- Dershowitz, W.S., Herda, H.H., 1992. Interpretation of fracture spacing and intensity, in: The 33rd US Symposium on Rock Mechanics (USRMS), OnePetro. URL: [https://doi.org/10.1016/0148-9062\(93\)91769-f](https://doi.org/10.1016/0148-9062(93)91769-f), doi:10.1016/0148-9062(93)91769-f.
475
- Ennes-Silva, R.A., Bezerra, F.H., Nogueira, F.C., Balsamo, F., Klimchouk, A., Cazarin, C.L., Auler, A.S., 2016. Superposed folding and associated fracturing influence hypogene karst development in Neoproterozoic carbonates, So Francisco Craton, Brazil. *Tectonophysics* 666, 244–259. URL: <https://linkinghub.elsevier.com/retrieve/pii/S0040195115006332>, doi:10.1016/j.tecto.2015.11.006.
480
- Ferronatto, J.P.F., dos Santos Scherer, C.M., Drago, G.B., Rodrigues, A.G., de Souza, E.G., dos Reis, A.D., Bállico, M.B., Kifumbi, C., Cazarin, C.L., 2021. Mixed carbonate-siliciclastic sedimentation in a mesoproterozoic storm-dominated ramp: Depositional processes and stromatolite development. *Precambrian Research* 361, 106240. URL: <https://doi.org/10.1016/j.precamres.2021.106240>, doi:10.1016/j.precamres.2021.106240.
485

- Figueiredo, F.T., De Almeida, R.P., Tohver, E., Babinski, M., Liu, D., Fanning, C.M., 2009. Neoproterozoic glacial dynamics revealed by provenance of diamictites of the Bebedouro Formation, São Francisco Craton, Central Eastern Brazil. *Terra Nova* 21, 375–385. URL: <https://doi.org/10.1111/j.1365-3121.2009.00893.x>, doi:10.1111/j.1365-3121.2009.00893.x.
- 490 Furtado, C.P., Medeiros, W.E., Borges, S.V., Lopes, J.A., Bezerra, F.H., Lima-Filho, F.P., Maia, R.P., Bertotti, G., Auler, A.S., Teixeira, W.L., 2022. The influence of subseismic-scale fracture interconnectivity on fluid flow in fracture corridors of the brejões carbonate karst system, brazil. *Marine and Petroleum Geology* 141, 105689. URL: <https://doi.org/10.1016/j.marpetgeo.2022.105689>, doi:10.1016/j.marpetgeo.2022.105689.
- 495 Girardeau-Montaut, D., 2022. CloudCompare. URL: <http://cloudcompare.org/>. version 2.12. Computer Software.
- Guadagnin, F., Chemale Jr, F., Magalhães, A.J., Santana, A., Dussin, I., Takehara, L., 2015. Age constraints on crystal-tuff from the Espinhaço SupergroupInsight into the Paleoproterozoic to Mesoproterozoic intracratonic basin cycles of the Congo–São Francisco Craton. *Gondwana Research* 27, 363–376. URL: <https://doi.org/10.1016/j.gr.2013.10.009>, doi:10.1016/j.gr.2013.10.009.
- 500 Guimaraes, J., Misi, A., Pedreira, A., Dominguez, J., 2011. The Bebedouro Formation, Una Group, Bahia (Brazil). *Geological Society, London, Memoirs* 36, 503–508. URL: <https://doi.org/10.1144/M36.47>, doi:10.1144/M36.47.
- Heilbron, M., Cordani, U.G., Alkmim, F.F., 2016. São Francisco Craton, Eastern Brazil: Tectonic Genealogy of a Miniature Continent. Springer. URL: <http://doi.org/10.1007/978-3-319-01715-0>, doi:10.1007/978-3-319-01715-0.
- Hodgetts, D., Drinkwater, N., Hodgson, J., Kavanagh, J., Flint, S., Keogh, K., Howell, J., 2004. Three-dimensional geological models from outcrop data using digital data collection techniques: an example from the tanqua karoo depocentre, south africa. *Geological Society, London, Special Publications* 239, 57–75. URL: <https://doi.org/10.1144/GSL.SP.2004.239.01.05>, doi:10.1144/GSL.SP.2004.239.01.05.
- 510 James, M.R., Robson, S., 2012. Straightforward reconstruction of 3d surfaces and topography with a camera: Accuracy and geoscience application. *Journal of Geophysical Research: Earth Surface* 117. URL: <https://doi.org/10.1029/2011JF002289>, doi:10.1029/2011JF002289.
- La Bruna, V., Bezerra, F.H., Souza, V.H., Maia, R.P., Auler, A.S., Araujo, R.E., Cazarin, C.L., Rodrigues, M.A., Vieira, L.C., Sousa, M.O., 2021. High-permeability zones in folded and faulted silicified carbonate rocks Implications for karstified carbonate reservoirs. *Marine and Petroleum Geology* 128, 105046. URL: <https://doi.org/10.1016/j.marpetgeo.2021.105046>, doi:10.1016/j.marpetgeo.2021.105046.

- Lopes, J.A.G., Medeiros, W.E., La Bruna, V., Lima, A., Bezerra, F.H.R., Schiozer, D.J., 2021. Advancements towards DFKN modelling: Incorporating fracture enlargement resulting from karstic dissolution in discrete fracture networks. *Journal of Petroleum Science and Engineering*, in revision process. URL: <https://www.sciencedirect.com/science/article/pii/S0920410521015588>, doi:10.1016/j.petrol.2021.109944.
- Magalhães, A., Scherer, C., Gabaglia, G.R., Bállico, M., Catuneanu, O., 2014. Unincised fluvial and tide-dominated estuarine systems from the Mesoproterozoic Lower Tombador Formation, Chapada Diamantina basin, Brazil. *Journal of South American Earth Sciences* 56, 68–90. URL: <https://doi.org/10.1016/j.jsames.2014.07.010>, doi:10.1016/j.jsames.2014.07.010.
- Martinelli, M., Bistacchi, A., Mittempergher, S., Bonneau, F., Balsamo, F., Caumon, G., Meda, M., 2020. Damage zone characterization combining scan-line and scan-area analysis on a km-scale digital outcrop model: The qala fault (gozo). *Journal of Structural Geology* 140, 104144. URL: <https://doi.org/10.1016/j.jsg.2020.104144>, doi:10.1016/j.jsg.2020.104144.
- Menegoni, N., Giordan, D., Perotti, C., 2020. Reliability and uncertainties of the analysis of an unstable rock slope performed on rpas digital outcrop models: The case of the gallivaggio landslide (western alps, italy). *Remote Sensing* 12, 1635. URL: <https://doi.org/10.3390/rs12101635>, doi:10.3390/rs12101635.
- Menezes, R.C.L., Loureiro, H.C., REIS, C., Santos, F.P.d., Miranda, D.A., Vieira, R., 2019. Carta geoligica: Folha Jacobina, SC-24-YC-III. Servio Geolgico do Brasil .
- Misi, A., Veizer, J., 1998. Neoproterozoic carbonate sequences of the Una Group, Irecê Basin, Brazil: chemostratigraphy, age and correlations. *Precambrian Research* 89, 87–100. URL: [https://doi.org/10.1016/S0301-9268\(97\)00073-9](https://doi.org/10.1016/S0301-9268(97)00073-9), doi:10.1016/S0301-9268(97)00073-9.
- Oliveira, R.G., Medeiros, W.E., 2018. Deep crustal framework of the Borborema Province, NE Brazil, derived from gravity and magnetic data. *Precambrian Research* 315, 45–65. URL: <https://doi.org/10.1016/j.precamres.2018.07.004>, doi:10.1016/j.precamres.2018.07.004.
- Pinto, M.S., Peucat, J., Martin, H., Sabaté, P., 1998. Recycling of the Archaean continental crust: the case study of the Gavião, State of Bahia, NE Brazil. *Journal of South American Earth Sciences* 11, 487–498. URL: [https://doi.org/10.1016/S0895-9811\(98\)00029-7](https://doi.org/10.1016/S0895-9811(98)00029-7), doi:10.1016/S0895-9811(98)00029-7.
- Pontes, C.C., Bezerra, F.H., Bertotti, G., La Bruna, V., Audra, P., De Waele, J., Auler, A.S., Balsamo, F., De Hoop, S., Pisani, L., 2021. Flow pathways in multiple-direction fold hinges: Implications for fractured and karstified carbonate reservoirs. *Journal of Structural Geology* 146, 104324. URL: <https://doi.org/10.1016/j.jsg.2021.104324>, doi:10.1016/j.jsg.2021.104324.
- Ramsay, J.G., 1967. *Folding and fracturing of rocks*. Mc Graw Hill Book Company 568.

- Santana, A., Chemale, F., Scherer, C., Guadagnin, F., Pereira, C., Santos, J.O.S., 2021. Paleogeographic
550 constraints on source area and depositional systems in the Neoproterozoic Irecê Basin, São Francisco
Craton. *Journal of South American Earth Sciences* 109, 103330. URL: <https://doi.org/10.1016/j.jsames.2021.103330>, doi:10.1016/j.jsames.2021.103330.
- Senger, K., Betlem, P., Birchall, T., Buckley, S.J., Coakley, B., Eide, C.H., Flraig, P.P., Forien, M., Galland,
555 O., Gonzaga Jr, L., et al., 2021. Using digital outcrops to make the high arctic more accessible through
the svalbox database. *Journal of Geoscience Education* 69, 123–137. URL: <https://doi.org/10.1080/10899995.2020.1813865>, doi:10.1080/10899995.2020.1813865.
- Senger, K., Betlem, P., Birchall, T., Gonzaga Jr, L., Grundvåg, S.A., Horota, R.K., Laake, A., Kuckero, L.,
560 Mørk, A., Planke, S., et al., 2022. Digitising svalbards geology: the festningen digital outcrop model. *First Break* 40, 47–55. URL: <https://doi.org/10.3997/1365-2397.fb2022021>, doi:10.3997/1365-2397.fb2022021.
- Souza, E.G.d., Scherer, C.M.S., dos Reis, A.D., Bállico, M.B., Ferronatto, J.P.F., Bofill, L.M., Kifumbi, C.,
565 2019. Sequence stratigraphy of the mixed wave-tidal-dominated Mesoproterozoic sedimentary succession
in Chapada Diamantina Basin, Espinhaço supergroup–Ne/Brazil. *Precambrian Research* 327, 103–120.
URL: <https://doi.org/10.1016/j.precamres.2019.03.007>, doi:10.1016/j.precamres.2019.03.007.
- Souza, V.H., Bezerra, F.H., Vieira, L.C., Cazarin, C.L., Brod, J.A., 2021. Hydrothermal silicification confined
570 to stratigraphic layers: Implications for carbonate reservoirs. *Marine and Petroleum Geology* 124, 104818.
URL: <https://doi.org/10.1016/j.marpetgeo.2020.104818>, doi:10.1016/j.marpetgeo.2020.104818.
- Srivastava, N.K., Rocha, A.J.D., 2002. Fazenda Cristal, BA - Estromatitos Mesoproterozoicos, in: Schobben-
haus, C., Campos, D.A., Queiroz, E.T., Winge, M., Berbert-Born, M.L.C. (Eds.), *Stios Geolgicos e Pale-*
ontolgicos do Brasil. Servio Geolgico do Brasil, Salvador(BA). chapter 11, pp. 87–93.
- Süssenberger, A., Neves, B.B.d.B., Wemmer, K., 2014. Dating low-grade metamorphism and deformation of
the Espinhaço Supergroup in the Chapada Diamantina (Bahia, NE Brazil): a K/Ar fine-fraction study.
Brazilian Journal of Geology 44, 207–220. URL: <https://doi.org/10.5327/Z2317-4889201400020003>,
doi:10.5327/Z2317-4889201400020003.
- Thiele, S.T., Grose, L., Samsu, A., Micklenthwaite, S., Vollgger, S.A., Cruden, A.R., 2017. Rapid, semi-
575 automatic fracture and contact mapping for point clouds, images and geophysical data. *Solid Earth* 8,
1241–1253. URL: <https://doi.org/10.5194/se-8-1241-2017>, doi:10.5194/se-8-1241-2017.
- Triantafyllou, A., Watlet, A., Le Mouélic, S., Camelbeeck, T., Civet, F., Kaufmann, O., Quinif, Y., Vandycque,
580 S., 2019. 3-d digital outcrop model for analysis of brittle deformation and lithological mapping (lorette
cave, belgium). *Journal of Structural Geology* 120, 55–66. URL: <https://doi.org/10.1016/j.jsg.2019.01.001>, doi:10.1016/j.jsg.2019.01.001.

Usman, M., Siddiqui, N.A., Zhang, S.Q., Mathew, M.J., Zhang, Y.X., Jamil, M., Liu, X.L., Ahmed, N., 2021. 3d geo-cellular static virtual outcrop model and its implications for reservoir petro-physical characteristics and heterogeneities. *Petroleum Science* 18, 1357–1369. URL: <https://doi.org/10.1016/j.petsci.2021.09.021>.

585 Warren, J., Root, P.J., 1963. The behavior of naturally fractured reservoirs. *Society of Petroleum Engineers Journal* 3, 245–255. URL: <https://doi.org/10.2118/426-PA>, doi:10.2118/426-PA.

List of Figures

590	1	Schematic diagram displaying the key features of the Integrative Model and its mutual connections.	24
600	2	A) Geologic and structural map of the area containing the studied Cristal Cave. B) Location map of the São Francisco Craton (SFC) and Cristal Cave relative positions. GIS data was obtained from Geological Survey of Brazil (CPRM) database (Menezes et al., 2019).	25
610	3	(A) Cartography of the Cristal Cave (Berbert-Born and Rocha, 1995), showing the location of Access 1 (in red). (B) and (C) show two visions of the geobody of the Access 1, that was composed from the photogrammetric model. (B) is a frontal view of the model, focusing in the main entrance of the cave., while (C) is the East view of the model, emphasizing the entrance morphology and the visualization of structural features.	26
620	4	Schematic stratigraphic chart of the Espinhaço and São Francisco Supergroups and their sub-units. Dashed lines refer to main unconformities and formation colors are the same shown in the geologic map. Ages are not to scale for visualization purposes. Adapted from Souza et al. (2019).	27
630	5	Relief map of the area containing the Cristal Cave overlaid with regional structures. Hillshade effect calculated from ALOS Palsar radar imagery. GIS data obtained from the Geological Survey of Brazil (SGB) database (Menezes et al., 2019).	28
640	6	Schematic model of fractures related to folding events. Highlighted zones refer to preferable pathways for fluid flow and for karst development, which include discontinuities such as fractures and slip interfaces. Modified from Ramsay (1967).	29
650	7	Side view of the Access 1 with the interpreted fracture sets. Red planes show interpreted fractures of the Group A, while greenish lines show interpreted traces of the Group B fractures.	30
660	8	Scale comparison of fracture traces interpreted from the DOM with field scanlines. The orange and green bars show the associated limits for virtual and field measurements, respectively.	31
670	9	Integrative plot of the columnar lithological section and petrophysical data. Data columns refer to porosity, permeability and elastic rebound (measured in horizontal and vertical directions). Reference levels that were used to tie the lithological section with the DOM are indicated as double gray lines.	32
680	10	Stereogram of the bedding attitudes measured virtually from the DOM of the Access 1. Note that the bedding planes of the west wall roughly dips westward, while the bedding planes of the east wall roughly dips to east. Outcrop photography illustrates the disposition of both walls with arrows markings the bedding and the interpreted fold axis.	33
690	11	A) Prismatic volume of the 3D Integrative Model. The photogrammetric model of the Access 1 is exhibited for scale and positioning purposes. Dashed lines identify the reference levels (marked in Figure 9) that were used to tie the lithological section to the DOM. B) 3D Lithological model composed of 22 layers. For each layer, petrophysical parameters can be assigned. In our case, we measured Porosity (C), Permeability (D), and Uniaxial Compressive Strength measurements both in horizontal (D) and vertical (E) directions. Data gaps are represented as shaded voids in the model. In (C)-(F), the horizontal bars show the density of measurements along depth.	34
700	12	Cross plots of the measured petrophysical parameters. The best-fit lines for each dataset are plotted in gray, with their respective correlation coefficient (r). For the Porosity versus Permeability plot, some outliers were removed for a better statistical representation. In the color scheme, warm colors represent the upper units (layers 14 to 22), while the blue color represents the lower units (layers 1 to 13).	35
710	13	(A) Stereogram of the fracture population mapped in the Access 1. (B) Rose diagram emphasizing the direction of those structures. Group A fractures are plotted in red, while Group B fractures are plotted in blue.	36
720	14	Examples of fractures present in the Access 1. (A) Large scale fracture with aperture parameter enlarged by dissolution process. (B) Stratabound fractures with millimetric aperture. Notice the absence of dissolution enlargement. (C) Small scale fractures and veins with silica and calcite infilling. The mini map shows the position of each photograph.	37

- 645 15 Stochastically generated DFN (A) and its intersection with simplified versions of the exposed surfaces of the cave in Access 1 (B-D). B, C, and D represent the ceiling, west wall and east wall, respectively. Fracture planes are represented as rectangular planes of constant thickness. In (A), the photogrammetric model is shown to scale and positioning reference. In (B-C), blues lines are intersections of the DFN with the respective planes and red lines are interpreted fracture traces from the DOM. Note that although individual fracture traces are not reproduced, P_{21} persistences are quite well similar in all surfaces.

650 16 Evolution of fracture aperture enlargement due to karstic dissolution. Following Lopes et al. (2021), in (A) the black line is a step-wise approximations of a power law relating fracture length and aperture, which is the starting phase (Stage I) of the dissolution process. Curve I is progressively changed such that, in the last stage of karstic dissolution (Stage IV), all apertures converge to the same value, regardless of fracture length. (B) shows the progressive evolution of the karstified fracture porosity. (C) and (D) show two intersections of the resulting DFKNs with the horizontal plane and the E-W vertical plane which pass close to the center of the Integrative Model. Note that the fracture aperture is reproduced in the width of the fracture traces.

655 17 Using the P_{21} persistence distribution inside the Integrative Model to delimit potential zones for cave development. (A) and (B) show two versions of the same horizontal slice, located near the center of the Integrative Model, where two zones of high intensity of P_{21} can be delimited. In (A), the delimited zone shows similar shape to the Access 1 itself while, in (B), the delimited zone presents the same overall appearance of the cave corridors. (C) and (D) compare the geobody delimited in (A) with the geobody of Access 1, respectively, while (E) and (F) compare the map of the zone delimited in (B) with the cave map in the area adjacent to Access 1, respectively. Note that the area delimited by the dashed rectangle in (F) is also shown in Figure 3A.

660 38 39 40

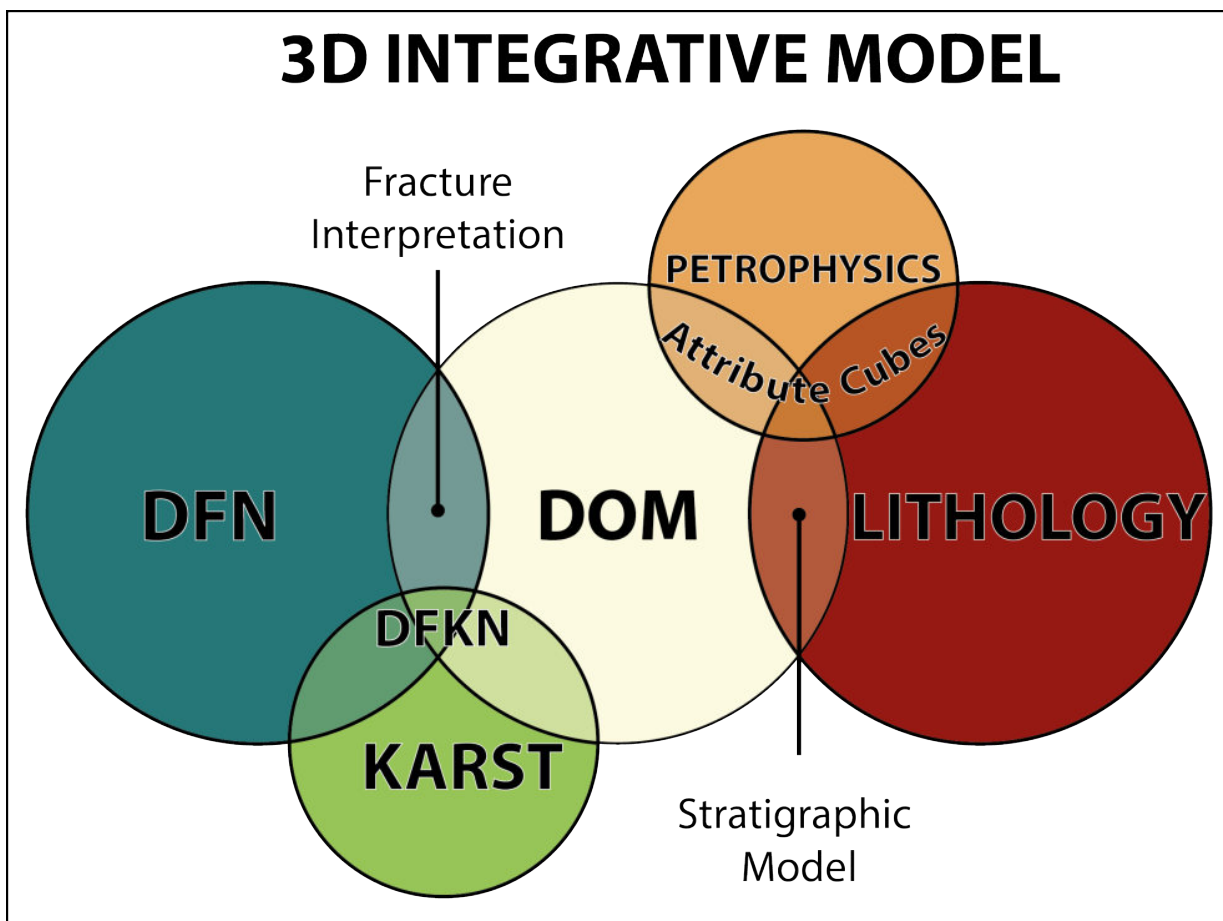


Figure 1: Schematic diagram displaying the key features of the Integrative Model and its mutual connections.

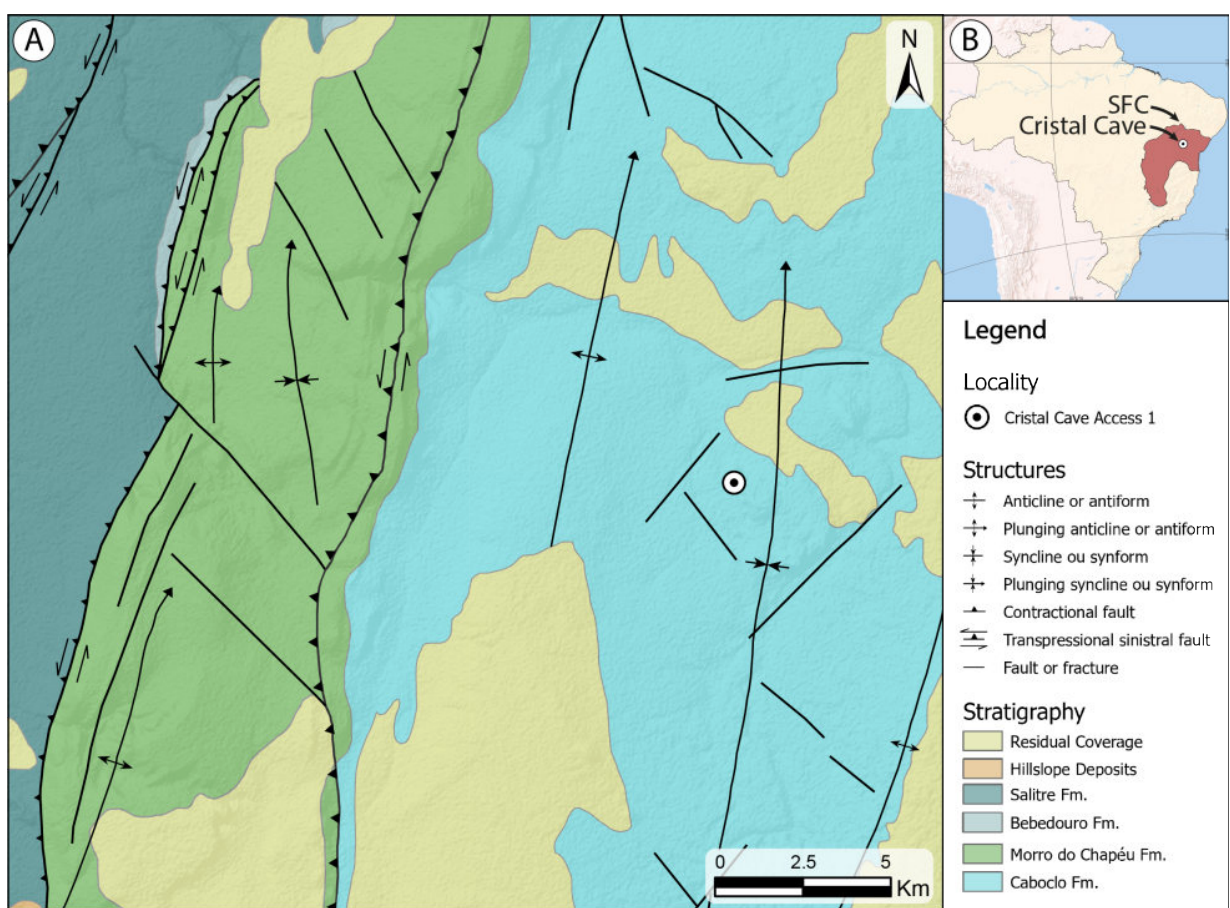


Figure 2: A) Geologic and structural map of the area containing the studied Cristal Cave. B) Location map of the São Francisco Craton (SFC) and Cristal Cave relative positions. GIS data was obtained from Geological Survey of Brazil (CPRM) database (Menezes et al., 2019).

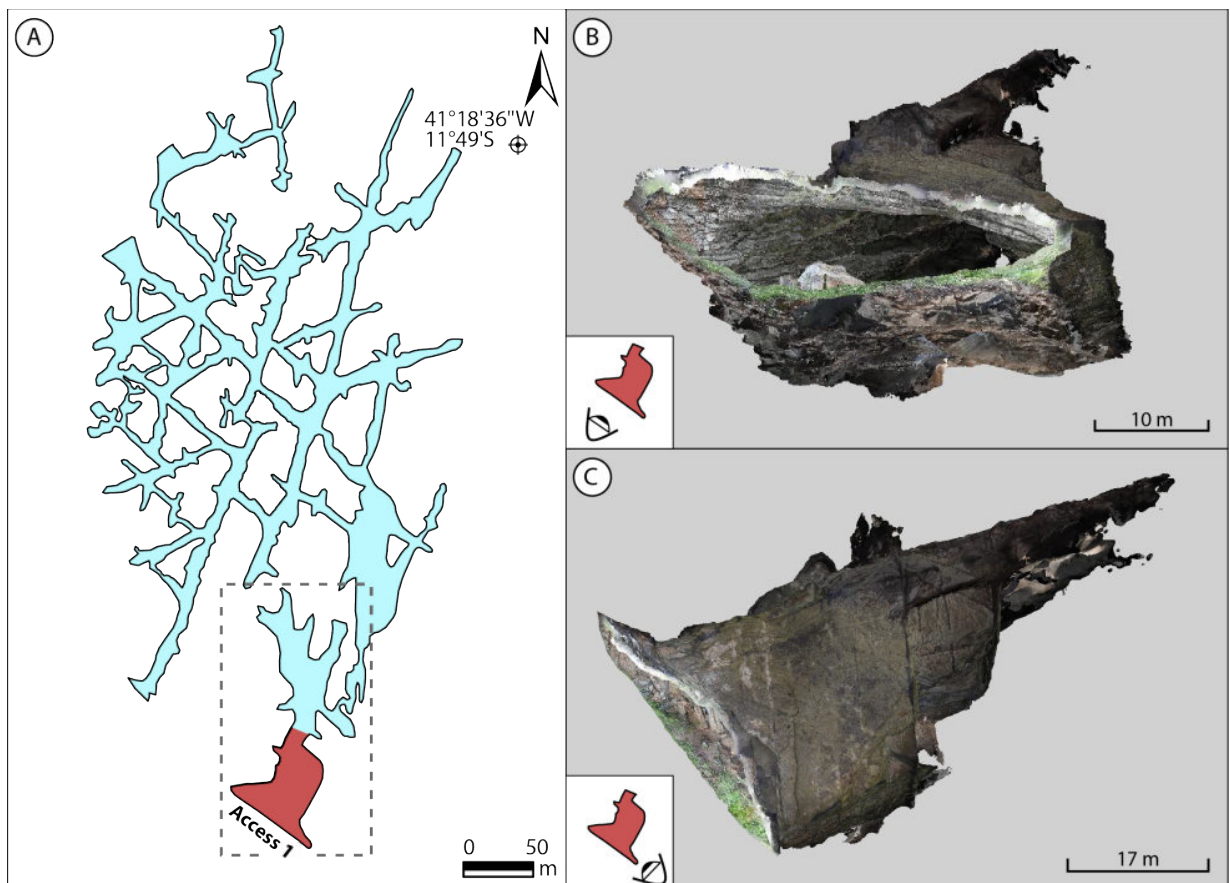


Figure 3: (A) Cartography of the Cristal Cave (Berbert-Born and Rocha, 1995), showing the location of Access 1 (in red). (B) and (C) show two visions of the geobody of the Access 1, that was composed from the photogrammetric model. (B) is a frontal view of the model, focusing in the main entrance of the cave., while (C) is the East view of the model, emphasizing the entrance morphology and the visualization of structural features.

Age	Era	Supergroup	Group	Megasequence	Formation
		Coverage (Fanerozoic)			
1.0 Ga	Neoproterozoic	São Francisco	Una		Salitre
					Bebedouro
				Upper	Morro do Chapéu
			Chapada Diamantina		Caboclo
		Espinhaço	Paraguaçu	Middle	Tombador
1.6 Ga	Mesoproterozoic				Açuruá
					Mangabeira
1.8 Ga	Paleoproterozoic		Rio dos Remédios	Lower	Lagoa de Dentro
					Novo Horizonte
					Serra da Gameleira
		Basement (Archean to Paleoproterozoic)			

Figure 4: Schematic stratigraphic chart of the Espinhaço and São Francisco Supergroups and their subunits. Dashed lines refer to main unconformities and formation colors are the same shown in the geologic map. Ages are not to scale for visualization purposes. Adapted from Souza et al. (2019).

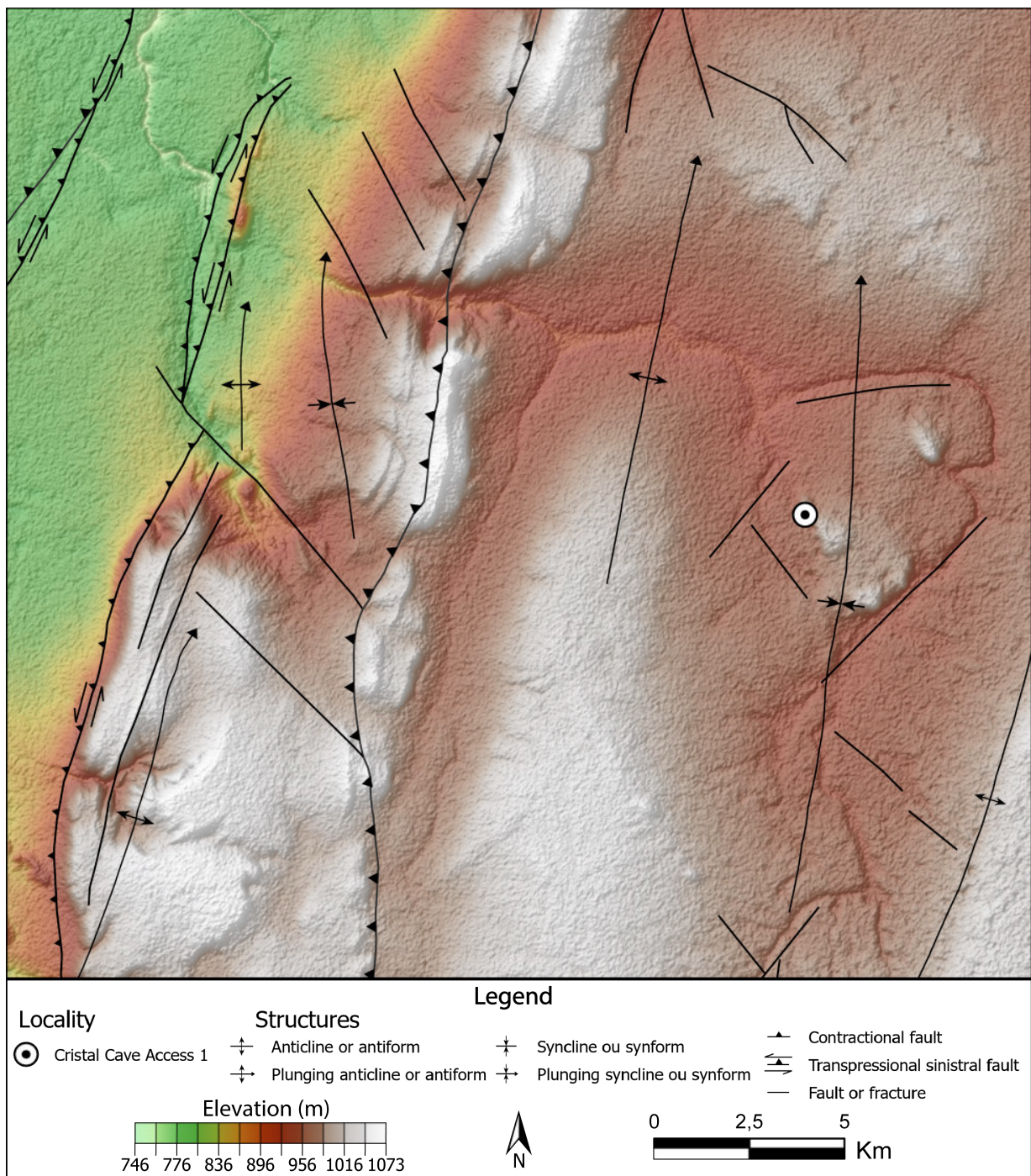


Figure 5: Relief map of the area containing the Cristal Cave overlaid with regional structures. Hillshade effect calculated from ALOS Palsar radar imagery. GIS data obtained from the Geological Survey of Brazil (SGB) database (Menezes et al., 2019).

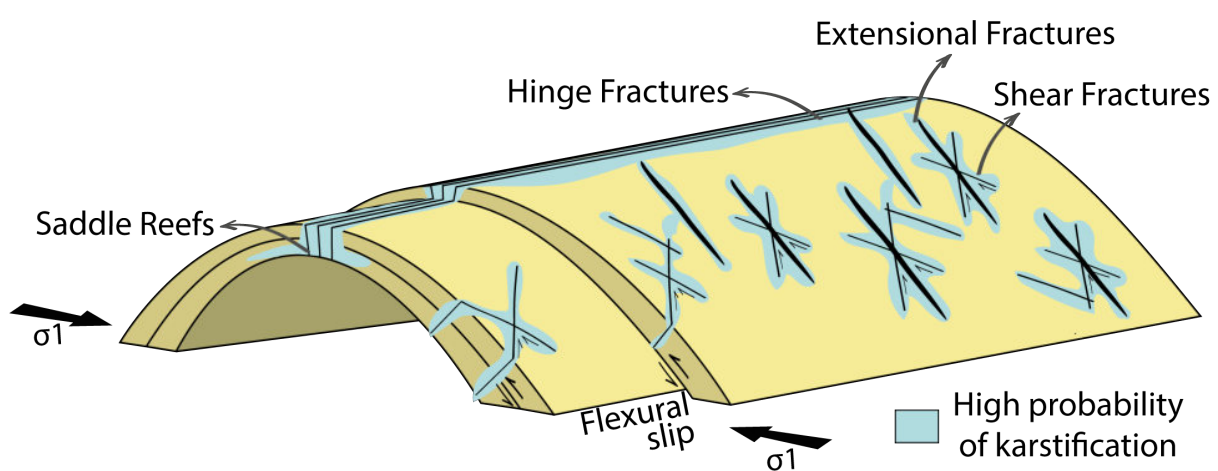


Figure 6: Schematic model of fractures related to folding events. Highlighted zones refer to preferable pathways for fluid flow and for karst development, which include discontinuities such as fractures and slip interfaces. Modified from Ramsay (1967).

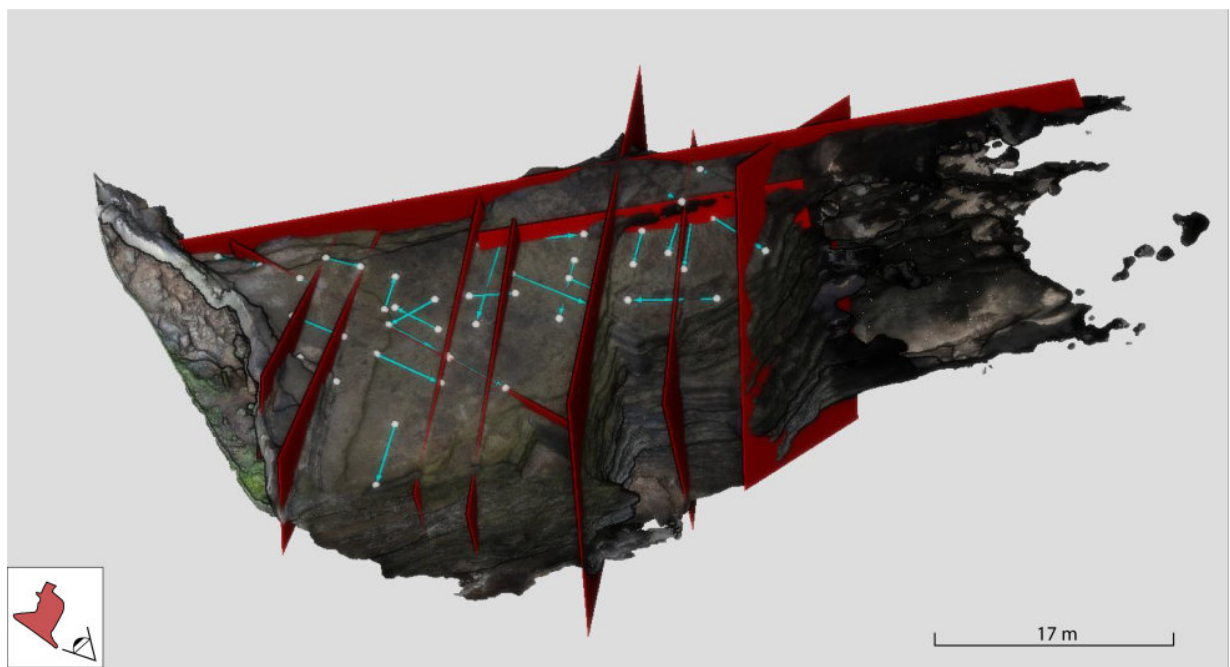


Figure 7: Side view of the Access 1 with the interpreted fracture sets. Red planes show interpreted fractures of the Group A, while greenish lines show interpreted traces of the Group B fractures.

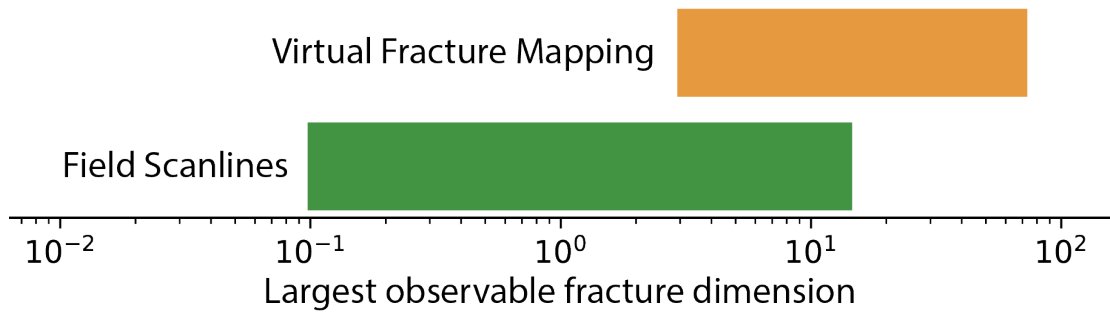


Figure 8: Scale comparison of fracture traces interpreted from the DOM with field scanlines. The orange and green bars show the associated limits for virtual and field measurements, respectively.

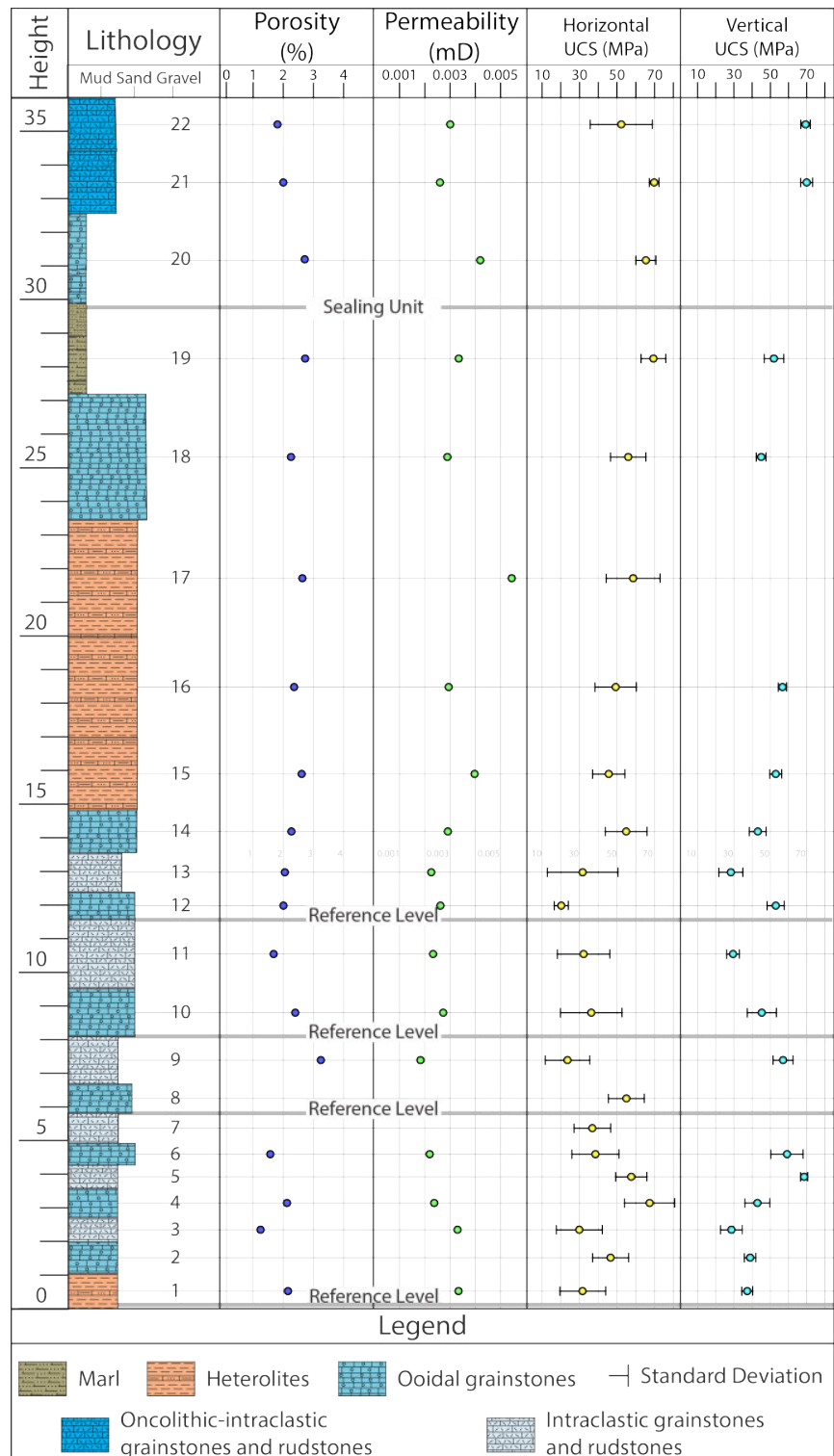


Figure 9: Integrative plot of the columnar lithological section and petrophysical data. Data columns refer to porosity, permeability and elastic rebound (measured in horizontal and vertical directions). Reference levels that were used to tie the lithological section with the DOM are indicated as double gray lines.

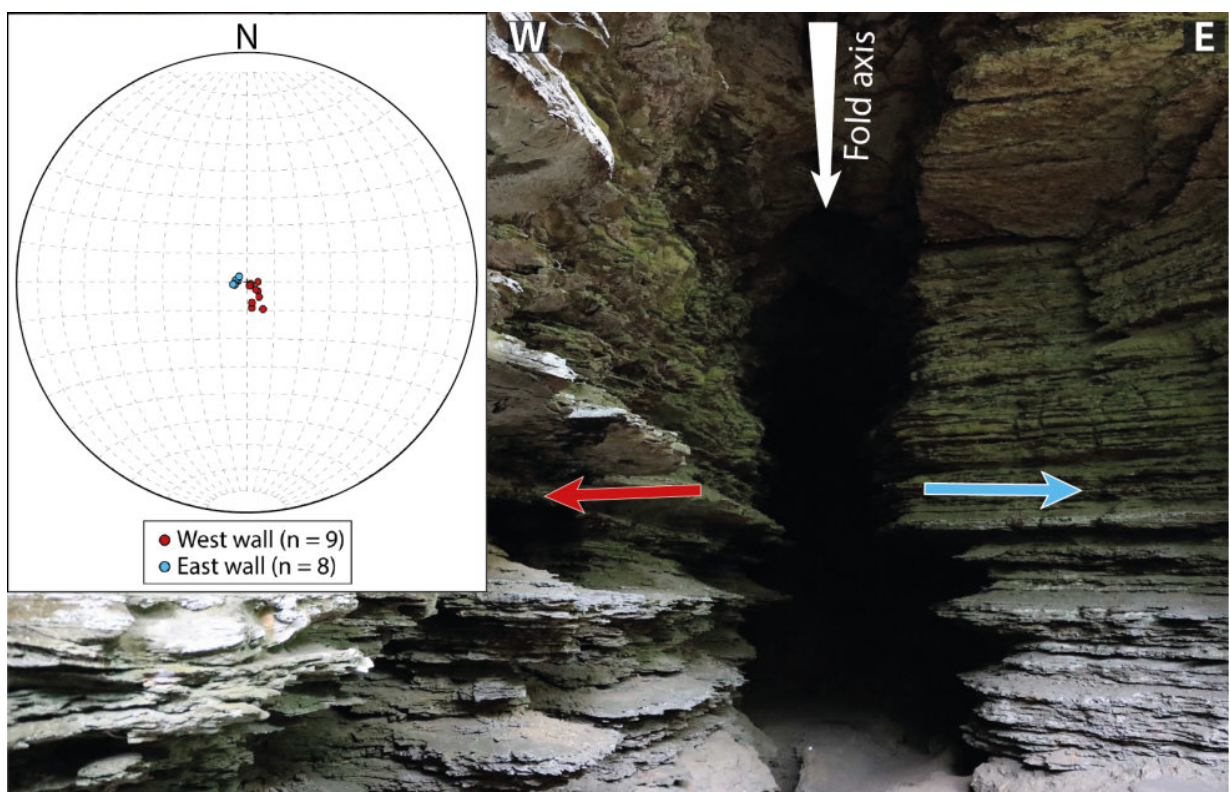


Figure 10: Stereogram of the bedding attitudes measured virtually from the DOM of the Access 1. Note that the bedding planes of the west wall roughly dips westward, while the bedding planes of the east wall roughly dips to east. Outcrop photography illustrates the disposition of both walls with arrows markings the bedding and the interpreted fold axis.

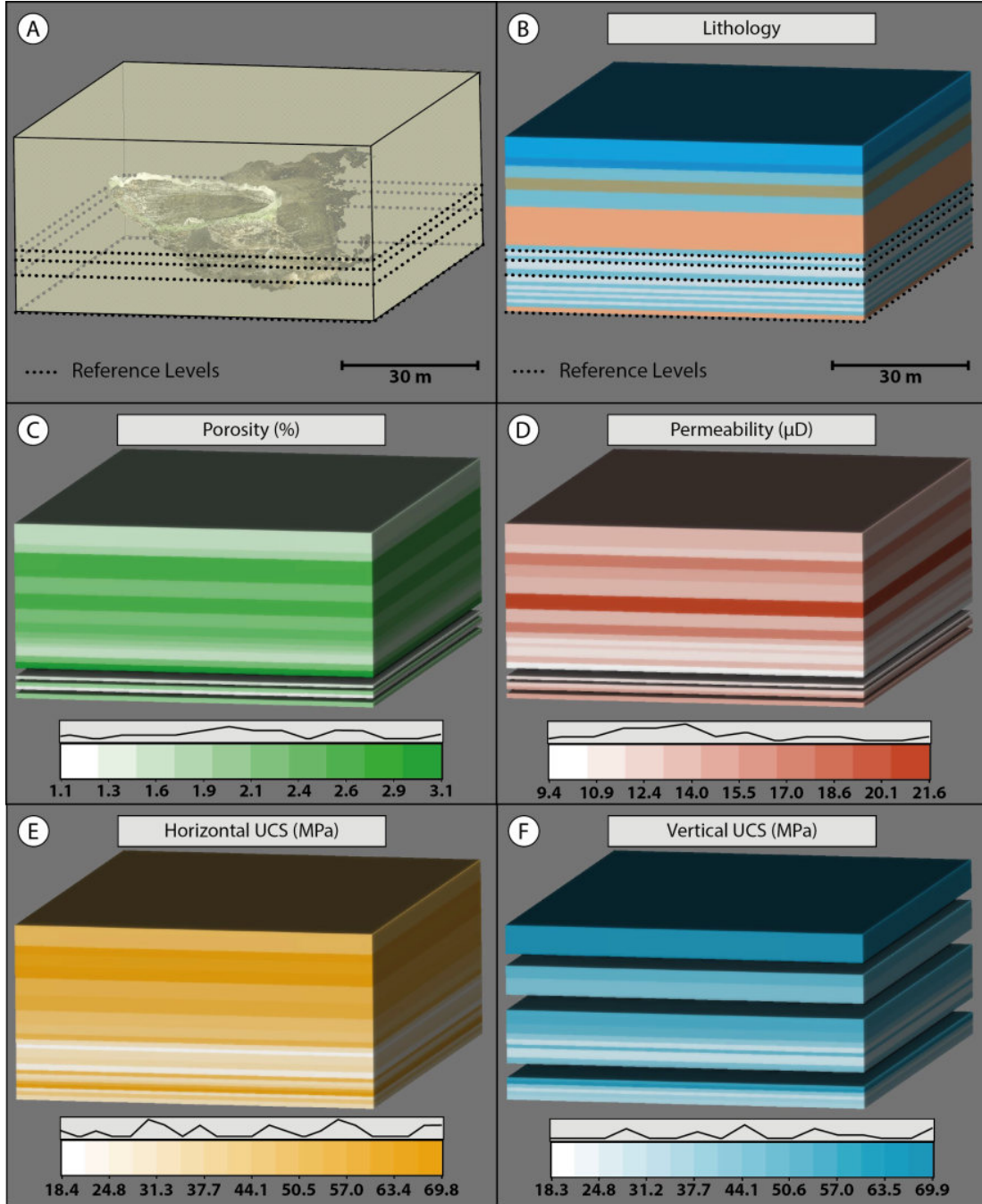


Figure 11: A) Prismatic volume of the 3D Integrative Model. The photogrammetric model of the Access 1 is exhibited for scale and positioning purposes. Dashed lines identify the reference levels (marked in Figure 9) that were used to tie the lithological section to the DOM. B) 3D Lithological model composed of 22 layers. For each layer, petrophysical parameters can be assigned. In our case, we measured Porosity (C), Permeability (D), and Uniaxial Compressive Strength measurements both in horizontal (D) and vertical (E) directions. Data gaps are represented as shaded voids in the model. In (C)-(F), the horizontal bars show the density of measurements along depth.

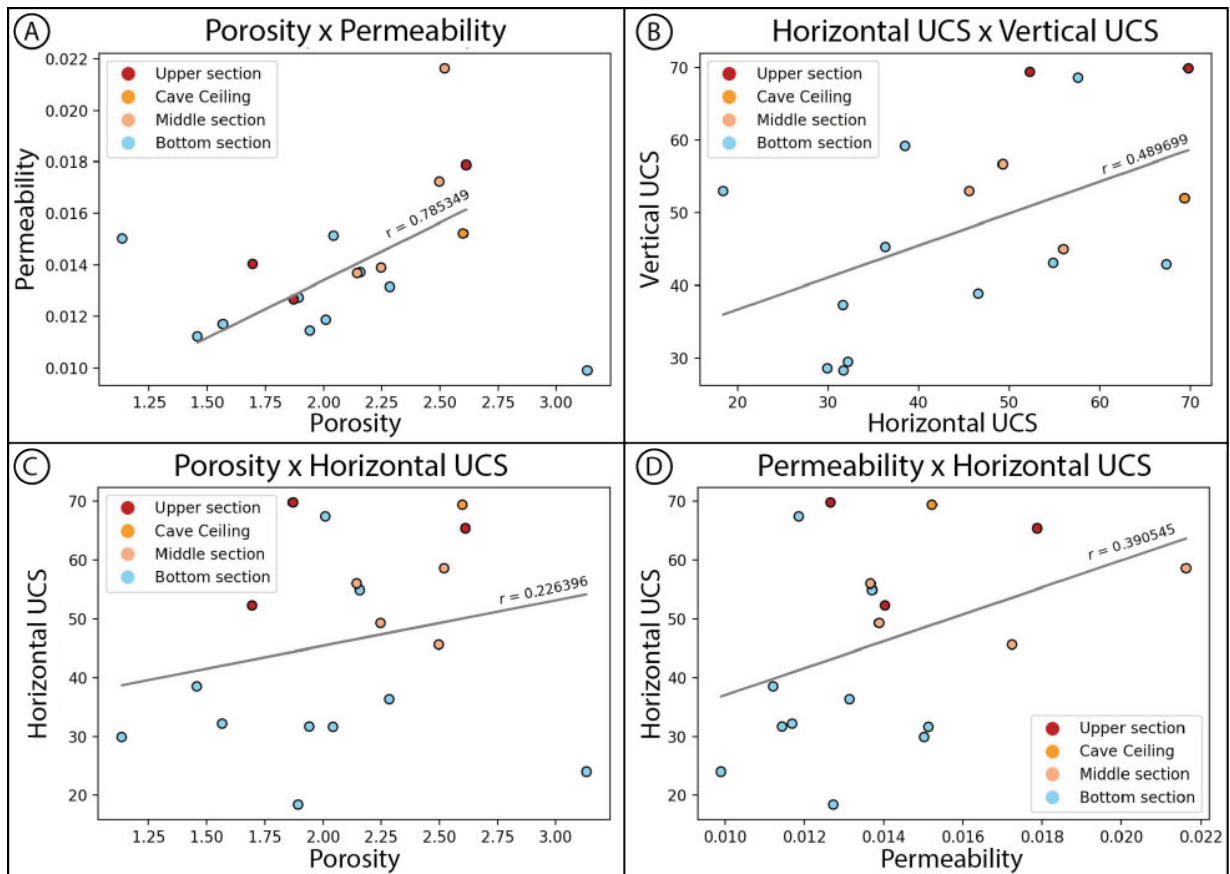


Figure 12: Cross plots of the measured petrophysical parameters. The best-fit lines for each dataset are plotted in gray, with their respective correlation coefficient (r). For the Porosity versus Permeability plot, some outliers were removed for a better statistical representation. In the color scheme, warm colors represent the upper units (layers 14 to 22), while the blue color represents the lower units (layers 1 to 13).

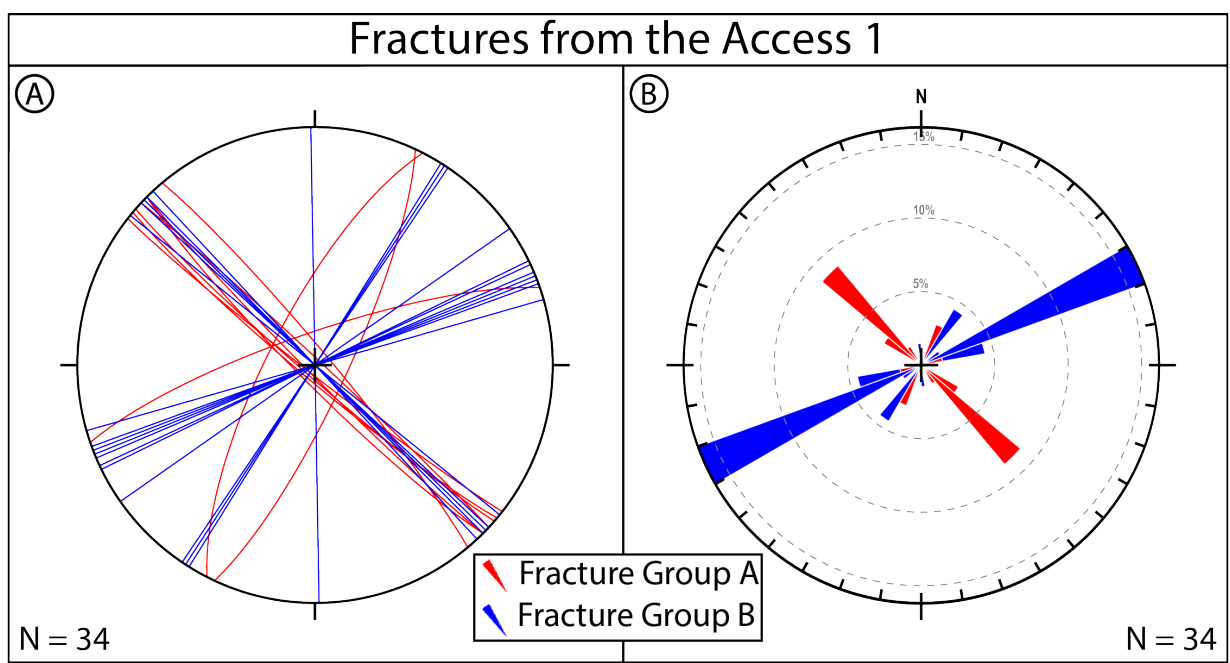


Figure 13: (A) Stereogram of the fracture population mapped in the Access 1. (B) Rose diagram emphasizing the direction of those structures. Group A fractures are plotted in red, while Group B fractures are plotted in blue.

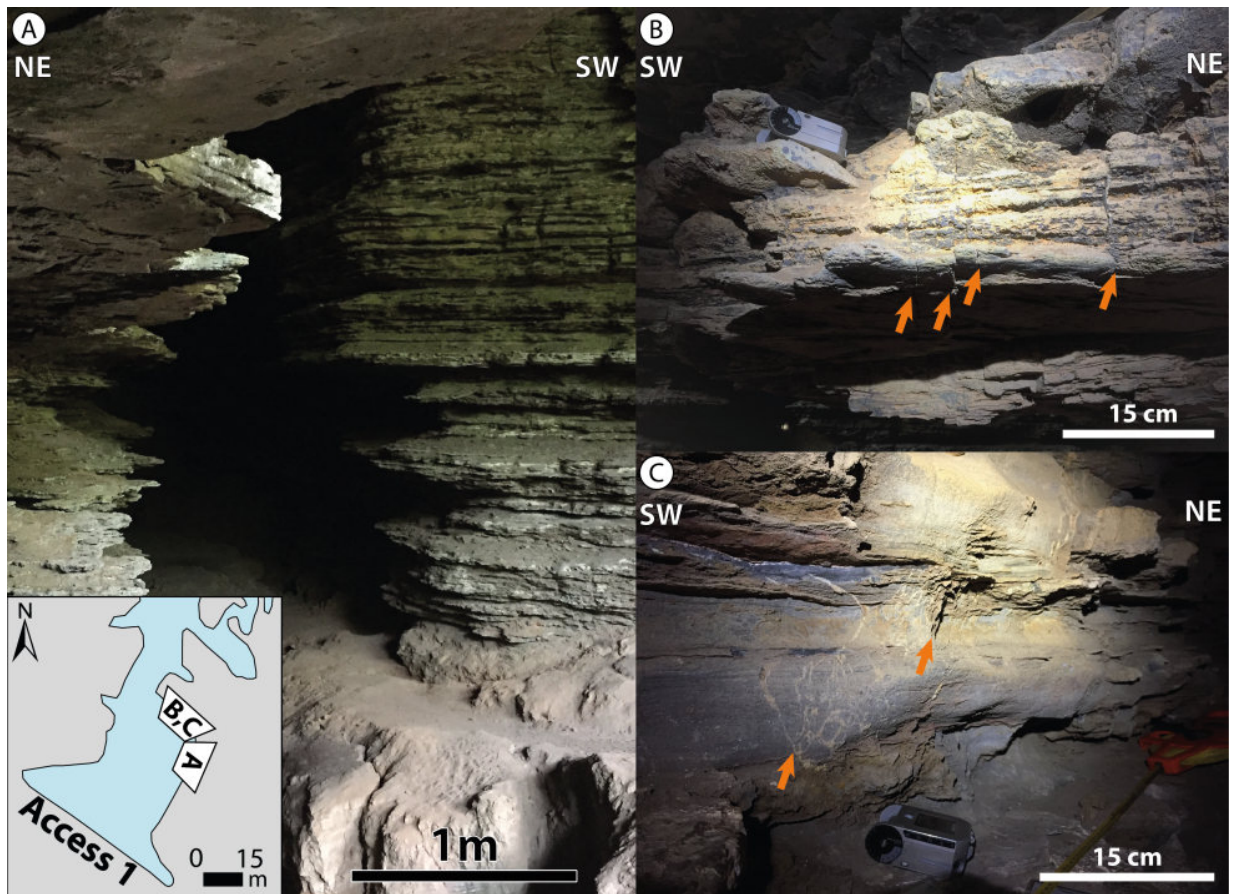


Figure 14: Examples of fractures present in the Access 1. (A) Large scale fracture with aperture parameter enlarged by dissolution process. (B) Stratabound fractures with millimetric aperture. Notice the absence of dissolution enlargement. (C) Small scale fractures and veins with silica and calcite infilling. The mini map shows the position of each photograph.

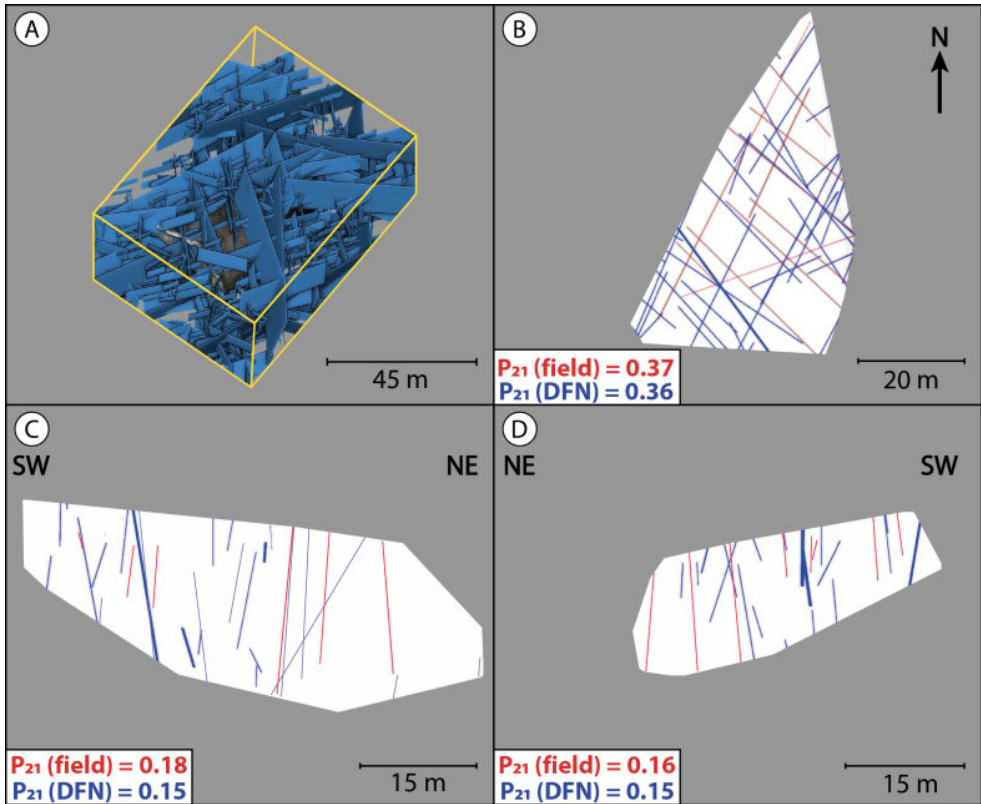


Figure 15: Stochastically generated DFN (A) and its intersection with simplified versions of the exposed surfaces of the cave in Access 1 (B-D). B, C, and D represent the ceiling, west wall and east wall, respectively. Fracture planes are represented as rectangular planes of constant thickness. In (A), the photogrammetric model is shown to scale and positioning reference. In (B-C), blues lines are intersections of the DFN with the respective planes and red lines are interpreted fracture traces from the DOM. Note that although individual fracture traces are not reproduced, P_{21} persistences are quite well similar in all surfaces.

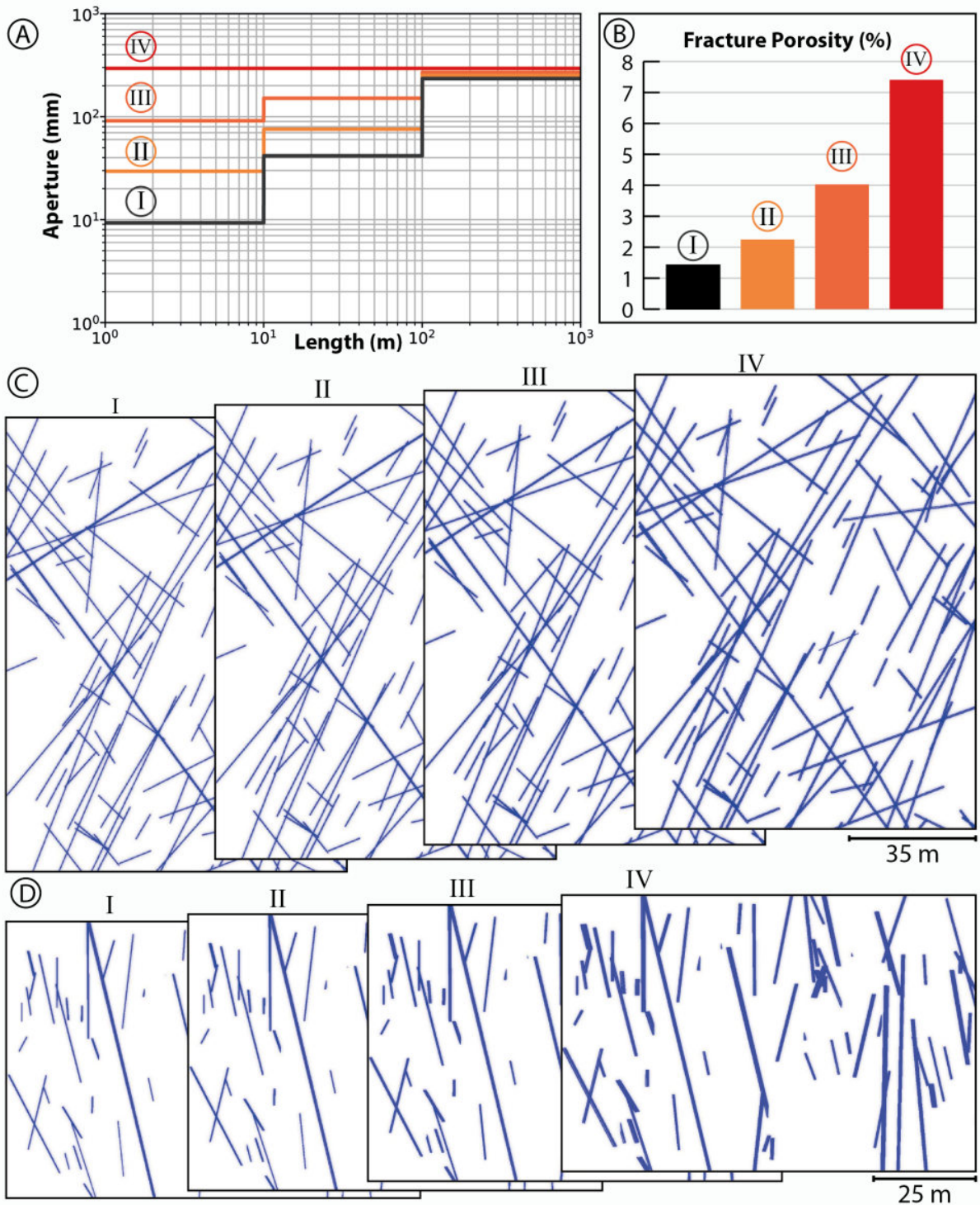


Figure 16: Evolution of fracture aperture enlargement due to karstic dissolution. Following Lopes et al. (2021), in (A) the black line is a step-wise approximations of a power law relating fracture length and aperture, which is the starting phase (Stage I) of the dissolution process. Curve I is progressively changed such that, in the last stage of karstic dissolution (Stage IV), all apertures converge to the same value, regardless of fracture length. (B) shows the progressive evolution of the karstified fracture porosity. (C) and (D) show two intersections of the resulting DFKNs with the horizontal plane and the E-W vertical plane which pass close to the center of the Integrative Model. Note that the fracture aperture is reproduced in the width of the fracture traces.

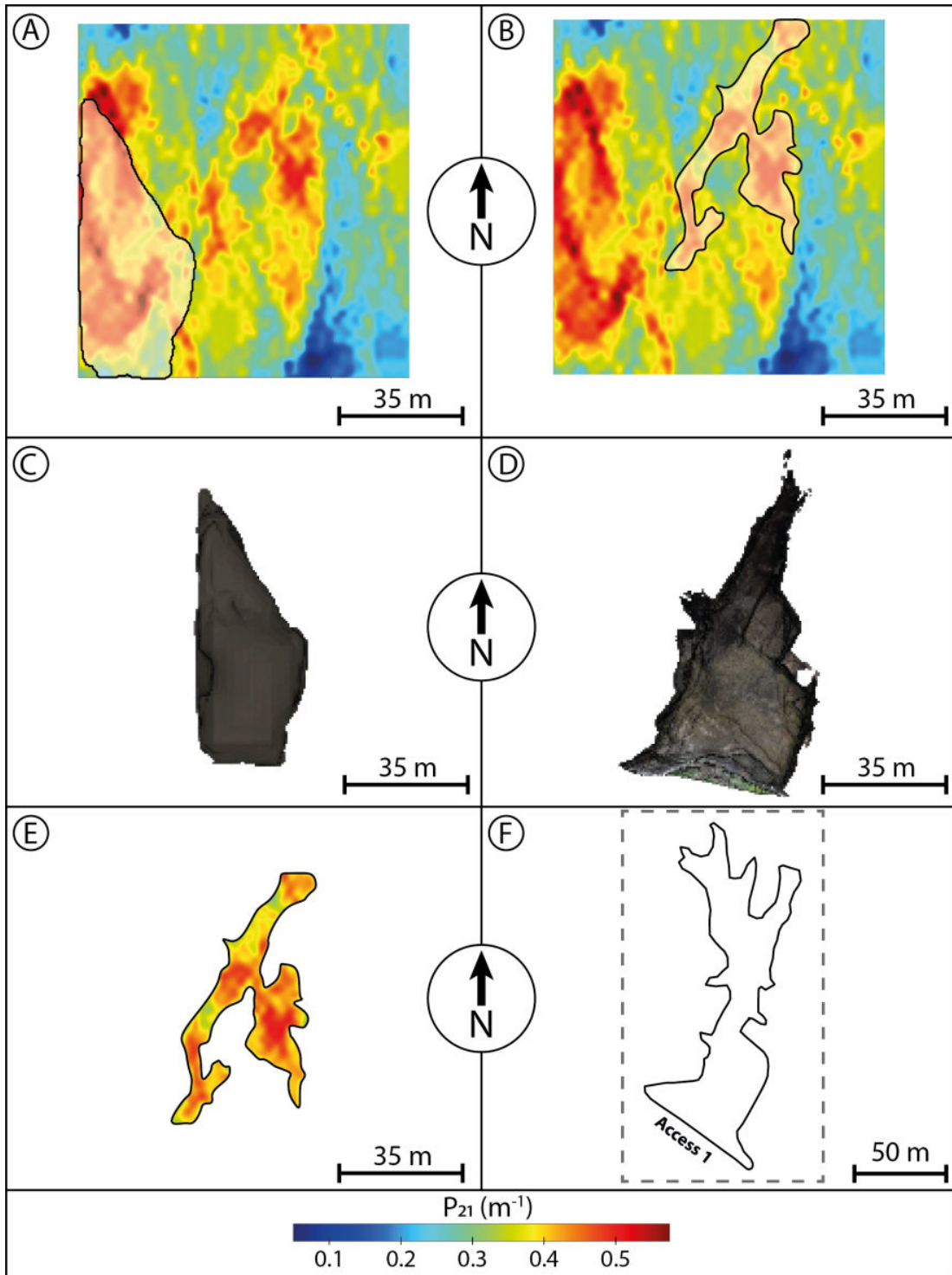


Figure 17: Using the P_{21} persistence distribution inside the Integrative Model to delimit potential zones for cave development. (A) and (B) show two versions of the same horizontal slice, located near the center of the Integrative Model, where two zones of high intensity of P_{21} can be delimited. In (A), the delimited zone shows similar shape to the Access 1 itself while, in (B), the delimited zone presents the same overall appearance of the cave corridors. (C) and (D) compare the geobody delimited in (A) with the geobody of Access 1, respectively, while (E) and (F) compare the map of the zone delimited in (B) with the cave map in the area adjacent to Access 1, respectively. Note that the area delimited by the dashed rectangle in (F) is also shown in Figure 3A.